Supporting Information for

Near Infrared Light Regulated Crystallization-Driven Self-Assembly: A Versatile Platform for Photo-Controlled Preparation of Uniform π-Conjugated Functional Nanostructures

Rang Chen,[a] *Sen Zhang*,[a] *Xiaoyu Huang*,[a,*] *Guolin Lu*,[a] *Mitchell A. Winnik*,[c,d] *Chun Feng*[a,b,*]

[a] State Key Laboratory of Fluorine and Nitrogen Chemistry and Advanced Materials, Shanghai Institute of Organic Chemistry, University of Chinese Academy of Sciences, 345 Lingling Road, Shanghai 200032, People's Republic of China

[b] Shanghai Key Laboratory of Advanced Polymeric Materials, School of Materials Science and Engineering, East China University of Science and Technology, 130 Meilong Road, Shanghai 200237, People's Republic of China

[c] Department of Chemistry, University of Toronto, 80 St. George St, Toronto, Ontario M5S 3H6, Canada

[d] Department of Chemical Engineering and Applied Chemistry, University of Toronto, Toronto, ON M5S 3E2

* To whom correspondence should be addressed, E-mail: cfeng@ecust.edu.cn (Tel: +86-21-54925606), xyhuang@mail.sioc.ac.cn (Tel: +86-21-54925310).

SUPPORTING EXPERIMENTAL DETAILS

Materials

2-Vinylpyridine (2VP, Aladdin, 97%) was passed through a basic alumina column and distilled under reduced pressure from CaH_2 prior to use. 2,2'-Azobis-(isobutyronitrile) (AIBN, 98%, Aldrich) was recrystallized from anhydrous ethanol. *N,N'*-Dicyclohexylcarbodiimide (DCC, Macklin, 99%), 4-dimethylaminopyridine (DMAP, Macklin, 99%), tris[(1-benzyl-1H-1,2,3-triazol-4-yl)methyl]amine (TBTA, Macklin, 97%), benzobisthiadiazole-based (BBT) compound 4-BBT-2Br (Macklin, 97%), bis(triphenylphosphine)palladium(II) chloride ($Pd(PPh_3)_2Cl_2$, TCI, 97%), copper(I) iodide (CuI, Aladdin, 99%), Indocyanine green (ICG, bidepharm, 97%), ethanol (EtOH, Macklin, ≥99.8%) and tetrabutyammonium fluoride (TBAF, TCI, 1.0 M in tetrahydrofuran) were used as received without further purification. All organic solvents such as dichloromethane (DCM), trimethylamine (TEA), toluene, tetrahydrofuran (THF) and *N,N*-dimethyformamide (DMF) were distilled prior to use. OPV_5-*b*-$P2VP_{42}$ was the same sample used in our previous report.[1] Other reagents not specially mentioned were purchased and used as received without further purification.

Instrumentation

Nuclear magnetic resonance (NMR)

^1H NMR analyses were performed on a JEOL JNM-ECZ 400 MHz or Bruker 500 MHz spectrometer in $CDCl_3$ or CD_2Cl_2, and chemical shifts were referenced to the residual solvent peak.

Gel permeation chromatography (GPC)

Relative molecular weights and molecular weight distributions were measured by conventional gel permeation chromatography (GPC) using a system equipped with a Waters 1515 Isocratic HPLC pump, a Waters 2414 refractive index detector, a Waters 2487 dual λ absorbance detector and a set of Waters Styragel columns (HR3 (500-30,000), HR4 (5,000-600,000) and HR5 (50,000-4,000,000), 7.8×300 mm, particle size: 5 μm). GPC measurements were carried out at 35°C using THF as eluent with a flow rate of 1.0 mL/min. The system was calibrated with linear polystyrene standards.

Matrix-assisted laser desorption/ionization time of flight mass spectrometry (MALDI-TOF-MS)

Small aliquots of sample solution (2 μL, 1.0 mg/mL) in CH_2Cl_2 were added to a sample plate for MALDI-TOF-MS measurement. After drying in air at room temperature (~10 min), an aliquot of α-cyano-4-hydroxy cinnamic acid (2 μL, 5.0 mg/mL) dispersed in a acetonitrile/water mixture ($V_{acetonitrile}/V_{water}$ = 1/1) was added and allowed to dry in air at room temperature. MALDI-TOF-MS spectra were obtained on a Bruker 7.0 T solarix MALDI spectrometer.

Transmission electron microscopy (TEM)

TEM images were obtained by a JEOL JEM-2100 instrument operated at 80 kV or 200 kV. A drop of micellar solution (10 μL) was placed on a Formvar and carbon-coated copper grid for 30 s and then a filter paper touched the edge of drop to absorb

most of liquid on the grid. The grid was allowed to dry at room temperature. For the samples stained by phosphotungstic acid, after the grid was dried (*ca*. 1 min after touching it with the filter paper), a drop of phosphotungstic acid aqueous solution (10 μL, 1.0 mg/mL) was added onto the surface. After 30 s, most of the solution on the grid was absorbed by touching the edge of the drop with a filter paper, and then the grid was allowed to dry at room temperature.

For each sample, length distribution of micelles was determined by tracing more than 100 individual micelles, and width distribution was determined by making measurements at least 100 different positions on several micelles and analysis using the ImageJ software program from National Institutes of Health. Number-average length (L_n), weight-average length (L_w), number-average width (W_n) and weight-average width (W_w) of micelles were calculated as follows:

$$\boldsymbol{L_n} = \frac{\sum_{i=1}^{N} N_i L_i}{\sum_{i=1}^{N} N_i} \quad (1)$$

$$\boldsymbol{L_w} = \frac{\sum_{i=1}^{N} N_i L_i^2}{\sum_{i=1}^{N} N_i L_i} \quad (2)$$

$$\boldsymbol{W_n} = \frac{\sum_{i=1}^{N} N_i W_i}{\sum_{i=1}^{N} N_i} \quad (3)$$

$$W_w = \frac{\sum_{i=1}^{N} N_i W_i^2}{\sum_{i=1}^{N} N_i W_i} \quad (4)$$

where N_i is the number of micelles of length L_i and width W_i, N is the number of calculated micelles in each sample. The distribution of micellar length and width is characterized by L_w/L_n, W_w/W_n and the standard deviation of length and width distribution σ.

Atomic force microscopy (AFM)

AFM images were acquired in air in tapping mode using a Bruker Dimension XR Spectrometer. Aliquots (10 μL) of micellar solution prepared as described below were deposited on a single-face-polished silicon wafer (ilabmarket) and dried at room temperature in air.

Circular dichroism (CD) measurements

CD spectra of micellar solution of 4-BBT-OPE$_3$-*b*-P2VP$_{22}$ (0.1 mg/mL in ethanol) were measured on a Chirascan V100 circular dichroism spectrophotometer over a wavelength range of 300-900 nm with a 1 nm resolution. Spectra were recorded three times using a 60 nm/min scanning speed (bandwidth: 1 nm). Spectrum of pure ethanol was used as baseline. Recorded traces were then baseline corrected and smoothed using the provided software.

Synchrotron-based grazing incident wide angle X-ray scattering (GIWAXS)

GIWAXS measurements were carried out on beamline BL14B1 in Shanghai Synchrotron Radiation Facility (SSRF). The incidence angle was 15° and beam energy was 10 keV. The tested film was prepared by casting the micellar solution of 4-BBT-OPE_7-*b*-$P2VP_{22}$ (1 mg/mL, in ethanol) onto a silicon wafer, and allowing it to dry at room temperature.

Steady state spectrometry

UV-vis-NIR absorption spectra were recorded on a Hitachi U-2910 spectrophotometer. Fluorescence emission spectra were measured by an Edinburgh FLS1000 photoluminescence spectrometer with a 10/20 nm excitation/emission band width. The conventional absorption and fluorescence measurements were performed at room temperature.

For the measurement of temperature-dependent UV-vis-NIR absorption spectra, the temperature of the cell housing (1 cm path cell) was controlled with a Neslab RTE-110 bath. The micellar samples (0.05 mg/mL in ethanol) were first heated at 70°C for 30 min, and then cooled to 20°C with a rate of ~0.5°C/min. After the solution was maintained at each target temperature for 3 min, UV-vis-NIR absorption spectra were recorded.

For the measurement of temperature-dependent fluorescence spectra, the micellar

samples (0.05 mg/mL in ethanol) were first heated at 70°C for 30 min, and then cooled to 20°C with a rate of ~0.5°C/min. After the solutions were maintained at each target temperature for 3 min, the fluorescence spectra were recorded.

Photoluminescence quantum yield

Absolute photoluminescence quantum yield (Φ_{PL}) was measured with an Edinburgh FLS1000 fluorescence spectrometer with an integrating sphere. Pure solvent (ethanol) and micellar solution of 4-BBT-OPE$_3$-*b*-P2VP$_{22}$ in a quartz cuvette (0.1 mg/mL, 2 mL in ethanol) were subjected to PLQY analysis. Φ_{PL} was calculated by the ratio of the number of emitted photons to the number of absorbed photons.[2] The following settings were used for the spectra acquisition: excitation wavelength 808 nm, excitation bandwidth 10 nm, detection wavelength range 780-1300 nm, emission bandwidth 10 nm, step 0.5 nm and dwell time 0.2 s.

Photothermal effect of micellar solution of 4-BBT-OPE$_3$-*b*-P2VP$_{22}$

Micellar solutions of 4-BBT-OPE$_3$-*b*-P2VP$_{22}$ in quartz cuvettes were exposed to NIR irradiation (808 nm laser) at different power densities (1.68, 1.22 and 0.82 W/cm^2). The temperature changes were monitored by a non-contact electronic thermometer probe (based on MLX90614 infrared temperature sensor) at an interval of 2 or 5 s over the irradiation process. For the examination of polymer content effect on photothermal activity, micellar solutions of 4-BBT-OPE$_3$-*b*-P2VP$_{22}$ with different contents were prepared (0.5, 0.2 and 0.1 mg/mL in ethanol, 0.22 mL), and exposed to NIR irradiation

(1.68 W/cm^2, 808 nm laser). The temperature changes were monitored by the non-contact electronic thermometer probe at an interval of 2 or 5 s over the irradiation process.

Calculation of photothermal conversion efficiency

The photothermal conversion efficiency (η) was calculated by the following formulas:[3, 4]

$$\eta = \frac{hA\Delta T_{max} - Q_s}{I(1 - 10^{-A_{808}})} \quad \text{(S1)}$$

$$\tau_s = \frac{m_i c_i}{hA} \quad \text{(S2)}$$

$$t = -\tau_s \ln(\theta) \quad \text{(S3)}$$

$$\theta = \frac{\Delta T}{\Delta T_{max}} \quad \text{(S4)}$$

$$Q_s = hA\Delta T_{EtOH} \quad \text{(S5)}$$

For calculating the photothermal conversion efficiency of micelles of 4-BBT-OPE$_3$-*b*-P2VP$_{22}$ (0.5 mg/mL, 1.68 W/cm^2), ΔT_{max} (°C) represents the maximum temperature change of micellar solution of 4-BBT-OPE$_3$-*b*-P2VP$_{22}$, which was obtained by Figure S29. Q_s expresses heat dissipated from light absorbed by solvent (ethanol). *I* expresses the incident laser power (power density × irradiation area = 1.68 W/cm^2 × 0.285 cm^2). A_{808} is the absorbance of 4-BBT-OPE$_3$-*b*-P2VP$_{22}$ micelles at 808 nm in ethanol (0.5 mg/mL, A_{808} = 0.983). *h* is the heat transfer coefficient and *A* is the surface area of the container. The mass of micellar solution (m_i) is 0.174 g, the heat capacity of ethanol (c_i) is 2.4 J g^{-1} K^{-1} and τ_s was calculated by eq. (S3) (Figure S29). *hA* was calculated

according to eq. (S2). The photothermal conversion efficiency (η) of 4-BBT-OPE_3-*b*-$P2VP_{22}$ micelles was calculated to be 24%.

Stability of micelles of 4-BBT-OPE_3-*b*-$P2VP_{22}$ against light irradiation

To evaluate the stability of micelles of 4-BBT-OPE_3-*b*-$P2VP_{22}$ against NIR or UV irradiation, micellar solution of 4-BBT-OPE_3-*b*-$P2VP_{22}$ (0.5 mg/mL in ethanol) in a quartz cuvette was exposed to NIR irradiation (808 nm 1.68 W/cm^2) for 22 min. The UV-vis-NIR absorption spectra of micellar solution before and after NIR irradiation were recorded using a Hitachi U-2910 spectrophotometer.

Micellar solution of 4-BBT-OPE_3-*b*-$P2VP_{22}$ (0.2 mg/mL in ethanol) in a quartz cuvette was also exposed to UV irradiation (390 nm, 0.05 W/cm^2) for 22 min. The absorption spectra of micellar solution before and after UV irradiation were also recorded using a Hitachi U-2910 spectrophotometer.

Simulation of possible packing modes of 4-BBT-OPE_3

To get more information about the packing mode of 4-BBT-OPE_3 units, simulations on two- and single-column octameric/tetrameric packing modes of 4-BBT-OPE_3, respectively, were run by Materials Studio 7.0 using Condensed-phase Optimized Molecular Potentials for Atomistic Simulation Studies (COMPASS) force field.[5, 6]

Construction of initial packing configuration

For different packing modes (two- or single-column), each model contains four

layers of molecules. The initial slipping angle between different layers was 90°, and the initial rotation angle was 0°. First, with the rotation angle set at 0°, each layer of molecules was translated a certain distance along the slipping direction to simulate the slipping between molecular layers. By adjusting different translation distances, a total of 20 initial packing configurations were obtained. Subsequently, the initial rotation angle was changed, and the above-mentioned translation process along the slipping direction were repeated. Finally, a total of 100 initial packing configurations were obtained with the slipping angles of these packing configurations from 30° to 90°, and the rotation angles from 0° to 2° (with an interval of 0.5°).

Energy of packing configuration calculation method

The simulations were run with the molecular modeling software package Materials Studio 7.0, using COMPASS force field.[5, 6] The COMPASS force field is an *ab initio* force field that enables accurate prediction of properties (structural, conformational, vibrational, *etc*.) for a broad range of organic molecules and polymers. The models were optimized to determine the minimum energy using a combined algorithm, namely smart algorithm, with a convergence level of 2×10^{-5} kcal/mol. The smart algorithm is a cascade of the steepest descent, ABNR (adjusted basis set Newton-Raphson) and quasi-Newton methods. For potential energy calculation, both Van der Waals and electrostatic force were computed using an atom-based summation method with a spline cutoff distance of 18.5 Å.

From an overlapping area perspective, the larger the overlapping area between

molecules, the more sufficient the interaction, and the more conducive it is to reduce the overall energy. For calculating the overlapping areas of two packing models. the Connolly method was used.[7, 8] The formula is as follows: overlapping area = (surface area of a single molecule) – (total surface area of molecular assembly/number of molecules).

Self-assembly Experiments

CDSA of 4-BBT-OPE$_3$-*b*-P2VP$_{22}$ in ethanol by heating/cooling protocol

A suspension of 4-BBT-OPE$_3$-*b*-P2VP$_{22}$ in ethanol (0.05 mg/mL) was heated at 80℃ in a water bath for 30 min and then cooled/aged at 25℃ (in a water bath set at 25℃) for 24 h. A drop of solution was placed on a carbon-coated copper grid and examined by TEM (Figures 2b, 2d and S19-20). AFM height images of 4-BBT-OPE$_3$-*b*-P2VP$_{22}$ micelles are presented in Figures 2e-f and S21.

Preparation of seed micelles of 4-BBT-OPE$_3$-*b*-P2VP$_{22}$

Seed micelles were prepared by a flash-freezing strategy instead of sonication approach to avoid sample degradation induced by the sonication.[9] A suspension of 4-BBT-OPE$_3$-*b*-P2VP$_{22}$ in ethanol (0.5 mg/mL) was heated at 80 ℃ for 40 min, and then cooled at -20 ℃ (in an ethanol cooling bath (cooler) set at -20 ℃) for 24 h. Seed micelles were examined by TEM (Figures 5b and S34) and kept below 15 ℃ for storing.

Direct heating regulated self-seeding of 4-BBT-OPE$_3$-*b*-P2VP$_{22}$

For the direct heating regulated self-seeding of 4-BBT-OPE_3-*b*-$P2VP_{22}$, aliquots of seed micelles of 4-BBT-OPE_3-*b*-$P2VP_{22}$ in ethanol (0.2, 0.1 and 0.05 mg/mL, diluted from the same seed micelles of 0.5 mg/mL, 0.22 mL) were heated in a water bath at different annealing temperatures for 30 min, the vials were removed from the bath and then cooled and aged at 25℃ (in a water bath set at 25℃) for 48 h. Finally, a drop of each solution was placed on a carbon-coated copper grid and examined by TEM (Figures S35, S37 and S39). Characterization details are summarized in Tables S5, S6 and S7.

NIR light regulated self-seeding of 4-BBT-OPE_3-*b*-$P2VP_{22}$

NIR light regulated self-seeding behaviour of 4-BBT-OPE_3-*b*-$P2VP_{22}$ with different contents (0.2, 0.1 and 0.05 mg/mL) was examined with a NIR laser (808 nm, 1.68 W/cm^2).

Aliquots of seed micelles of 4-BBT-OPE_3-*b*-$P2VP_{22}$ (0.2, 0.1 and 0.05 mg/mL, diluted from the above-described seed micelles of 0.5 mg/mL, 0.22 mL) were subjected to NIR laser irradiation for different times when the temperature of solution reached about 32℃, 33℃, 34℃, 35℃, 36℃, 37℃, 38℃, 39℃ and 40℃, respectively, from an initial temperature of 26℃. After the temperature reached the target value, the solutions were cooled in air and aged at 25℃ (in a water bath set at 25℃) for 48 h. Finally, a drop of each solution was placed on a carbon-coated copper grid and examined by TEM (Figures S36, S38 and S40). Characterization details are summarized in Tables S2, S3 and S4.

To investigate the influence of NIR laser power on NIR regulated self-seeding, aliquots of seed micelles of 4-BBT-OPE_3-*b*-$P2VP_{22}$ (0.22 mL, 0.1 mg/mL) in ethanol at 26°C were subjected to NIR laser irradiation with powers of 1.68, 1.22, 0.82 and 0.64 W/cm^2 for different times when the temperatures of the solutions reached about 35°C, 37°C and 39°C, respectively. After the temperature reached the target value, the solutions were cooled/aged at 25°C (in a water bath set at 25°C) for 48 h. Finally, a drop of each solution was placed on a carbon-coated copper grid and examined by TEM (Figures S43). Characterization details are summarized in Table S8.

Preparation of seed micelles of OPV_5-*b*-$P2VP_{42}$

First, a suspension of OPV_5-*b*-$P2VP_{42}$ (0.05 mg/mL in ethanol, 5 mL) was heated at 80°C, followed by cooling/aging at 25°C (in a water bath set at 25°C) for 24 h. Subsequently, the micellar solution was subjected to mild sonication (BRANSON 1510 ultrasonic cleaning bath, 70 W) to give seed micelles (Figure S48, L_n = 44 nm, L_w/L_n = 1.10, 0.05 mg/mL).

Direct heating regulated self-seeding of OPV_5-*b*-$P2VP_{42}$

For the direct heating regulated self-seeding of OPV_5-*b*-$P2VP_{42}$, aliquots of seed micelles of OPV_5-*b*-$P2VP_{42}$ in ethanol (Figure S48, L_n = 44 nm, L_w/L_n = 1.10, 0.05 mg/mL, 0.22 mL) were heated at different annealing temperatures for 30 min. Then the vials were removed from the bath and allowed to cool in air and finally aged at 25°C (in a water bath set at 25°C) for 48 h. A drop of each solution was placed on a carbon-

coated copper grid and examined by TEM (Figures S49a-f). Characterization details are summarized in Tables S10.

NIR light regulated self-seeding of OPV_5-*b*-$P2VP_{42}$

NIR light regulated self-seeding behaviour of OPV_5-*b*-$P2VP_{42}$ in the presence of ICG was examined. Aliquots of seed micelles of OPV_5-*b*-$P2VP_{42}$ (Figure S48, L_n = 44 nm, L_w/L_n = 1.10, 0.05 mg/mL in ethanol, 0.22 mL) in the presence of ICG (0.01 mg/mL) were subjected to NIR laser irradiation (808 nm, 1.68 W/cm^2) for of 20 s, 28 s, 40 s, 58 s and 112 s to let the temperature of the solutions reach 35 ^{o}C, 40 ^{o}C, 45 ^{o}C, 50 ^{o}C and 55 °C, respectively. After the temperature reached the target value, the solutions were cooled/aged at 25°C (in a water bath set at 25°C) for 48 h. Finally, a drop of each solution was placed on a carbon-coated copper grid and examined by TEM (Figures 6 and S49g-l). Characterization details are summarized in Tables S11.

NIR light regulated self-seeding of 4-BBT-OPE_3-*b*-$P2VP_{22}$ in the presence of blocking biological tissue

Aliquots of seed micelles of 4-BBT-OPE_3-*b*-$P2VP_{22}$ (0.22 mL, 0.1 mg/mL) were placed under slices of chicken breast tissue with different thickness (1, 2, 3 and 4 mm, the experimental setup is shown in Figure S44) for laser irradiation (808 nm, 1.68 W/cm^2) with varying times to let the solution temperature reach 38°C. After the temperature reached the target value, the solutions were allowed to cool in air and aged at 25°C (in a water bath set at 25°C) for 48 h. Finally, a drop of each solution was placed

on a carbon-coated copper grid and examined by TEM (Figures 7d-g). Characterization details are summarized in Table S9.

After the laser passed through different pieces of chicken tissue with different thicknesses (1, 2, 3 and 4 mm), the output ("working") power of the 808 nm laser with an input power of 1.68 W/cm^2 was measured using an optical power meter (purchased from Beijing Perfectlight Co., Ltd., China).

Monomer and Polymer Synthesis

Synthesis of asymmetric OPE_3

OPE_3 was synthesized via a modified reported procedure (Scheme S1).[10]

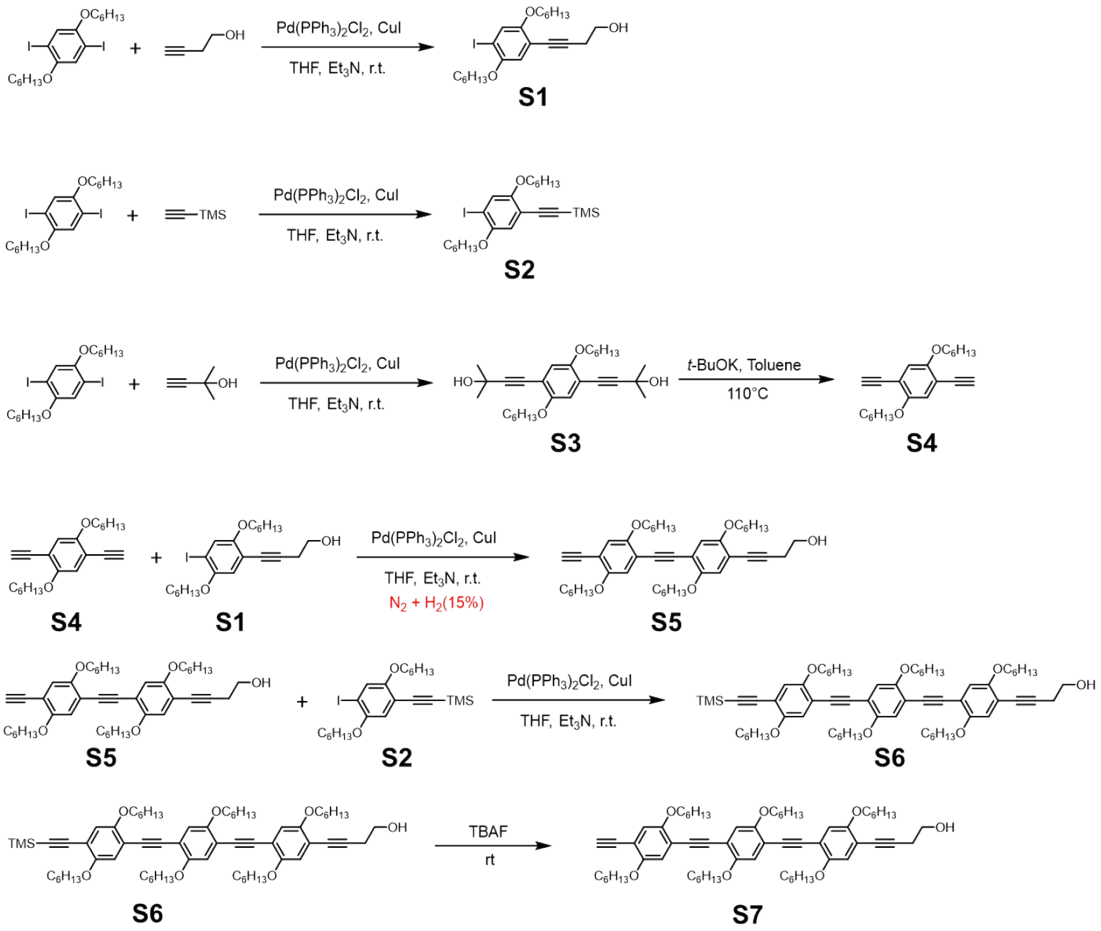

Scheme S1. Synthetic route of OPE_3.

Synthesis of S1

$[Pd(PPh_3)_2Cl_2]$ (442.2 mg, 0.63 mmol, 0.05 eq.), CuI (47.6 mg, 0.25 mmol, 0.02 eq.) and 1,4-bis(hexyloxy)-2,5-diiodobenzene (10.00 g, 18.86 mmol, 1.50 eq.) were added into a 250 mL Schlenk flask, followed by degassing, and the mixture was kept under N_2. Next, THF (50 mL) and triethylamine (20 mL) were added via a gastight syringe. The solution was bubbled with N_2 for 30 min, followed by adding 3-butyn-2-ol (881.0

mg, 12.57 mmol, 1.00 eq.). After the reaction mixture was stirred at room temperature under N_2 overnight, the solvent was evaporated *in vacuo* and the crude product was purified by silica column chromatography (DCM:hexane = 1:4 to 4:1, v/v) to give **S1** as a yellow liquid (4.16 g, 70%).

^{1}H NMR (400 MHz, $CDCl_3$): δ (ppm): 0.84-0.98 (m, 6H, $OCH_2(CH_2)_4CH_3$), 1.28-1.39 (m, 8H, $OCH_2CH_2CH_2(CH_2)_2CH_3$), 1.40-1.56 (m, 4H, $OCH_2CH_2CH_2(CH_2)_2CH_3$), 1.79 (m, 4H, $OCH_2CH_2CH_2(CH_2)_2CH_3$), 2.71 (t, J = 6.1 Hz, 2H, CH_2CH_2OH), 3.80 (t, J = 6.1 Hz, 2H, CH_2CH_2OH), 3.93 (m, 4H, $OCH_2CH_2CH_2(CH_2)_2CH_3$), 6.80 (s, 1H, Ar*H*), 7.25 (s, 1H, Ar*H*).

Synthesis of S2

$[Pd(PPh_3)_2Cl_2]$ (1.32 g, 1.89 mmol, 0.05 eq.), CuI (143.7 mg, 0.75 mmol, 0.02 eq.) and 1,4-bis(hexyloxy)-2,5-diiodobenzene (20.00 g, 37.72 mmol, 1.00 eq.) were added into a 500 mL Schlenk flask, followed by degassing, and the mixture was kept under N_2. Next, THF (150 mL) and triethylamine (50 mL) were added via a gastight syringe. The solution was bubbled with N_2 for 30 min followed by adding trimethylsilylacetylene (4.82 g, 6.93 mL, 49.04 mmol, 1.30 eq.). After the reaction mixture was stirred at room temperature under N_2 overnight, the solution was filtered and the solvent was evaporated *in vacuo*. The crude product was purified by silica column chromatography (DCM:hexane = 1:100 to 1:50, v/v) to give **S2** as a yellow solid (12.71 g, 67%).

^{1}H NMR (400 MHz, CD_2Cl_2): δ (ppm): 0.24 (s, 9H, $Si(CH_3)_3$), 0.84-0.96 (m, 6H,

$OCH_2CH_2CH_2(CH_2)_2CH_3$), 1.29-1.40 (m, 8H, $OCH_2CH_2CH_2(CH_2)_2CH_3$), 1.43-1.54 (m, 4H, $OCH_2CH_2CH_2(CH_2)_2CH_3$), 1.71-1.84 (m, 4H, $OCH_2CH_2CH_2(CH_2)_2CH_3$), 3.93 (t, 4H, $OCH_2CH_2CH_2(CH_2)_2CH_3$), 6.83 (s, 1H, Ar*H*), 7.28 (s, 1H, Ar*H*).

Synthesis of S3

$[Pd(PPh_3)_2Cl_2]$ (1.32 g, 1.89 mmol, 0.05 eq.), CuI (0.36 g, 1.89 mmol, 0.05 eq.) and 1,4-bis(hexyloxy)-2,5-diiodobenzene (20.00 g, 37.72 mmol, 1.00 eq.) were added into a 500 mL Schlenk flask, followed by degassing, and the mixture was kept under N_2. Next, THF (200 mL) and triethylamine (100 mL) were added via a gastight syringe. The solution was bubbled with N_2 for 30 min followed by adding 2-methyl-3-butyn-2-ol (3.81 g, 45.26 mmol, 1.20 eq.). After the reaction mixture was stirred at room temperature under N_2 overnight, the solvent was evaporated *in vacuo* and the crude product was purified by silica column chromatography (DCM:EA = 20:1 to 5:1, v/v) to give **S3** as a light brown solid (6.29 g, 38%).

^{1}H NMR (400 MHz, $CDCl_3$): δ (ppm): 0.86-0.94 (m, 6H, $OCH_2(CH_2)_4CH_3$), 1.28-1.39 (m, 8H, $OCH_2CH_2CH_2(CH_2)_2CH_3$), 1.44-1.54 (m, 4H, $OCH_2CH_2CH_2(CH_2)_2CH_3$), 1.62 (s, 12H, $C(CH_3)_2$), 1.78 (m, 4H, $OCH_2CH_2CH_2(CH_2)_2CH_3$), 2.01 (br., O*H*), 3.93 (t, J = 6.4 Hz, 4H, $OCH_2CH_2CH_2(CH_2)_2CH_3$), 6.85 (s, 1H, Ar*H*).

Synthesis of S4

S3 (5.00 g, 11.30 mmol, 1.00 eq.) and *t*-BuOK (3.80 g, 33.90 mmol, 3.00 eq.) were added into a 500 mL round-bottom flask, and then 180 mL of toluene was added,

followed by stirring at 110°C for 0.5 h. After the reaction was complete, the flask was quickly cooled to terminate the reaction. After the reaction mixture was diluted with DCM and filtered over celite to remove solid impurities, the solvent was evaporated *in vacuo* and the crude product was purified by silica column chromatography (DCM: hexane = 1:10 to 1:2, v/v) to give **S4** as a light-yellow solid (2.92 g, 79%).

^{1}H NMR (400 MHz, $CDCl_3$): δ (ppm): 0.86-0.94 (m, 6H, $OCH_2(CH_2)_4CH_3$), 1.28-1.39 (m, 8H, $OCH_2CH_2CH_2(CH_2)_2CH_3$), 1.41-1.52 (m, 4H, $OCH_2CH_2CH_2(CH_2)_2CH_3$), 1.80 (m, 4H, $OCH_2CH_2CH_2(CH_2)_2CH_3$), 3.33 (s, 1H, alkyne *H*), 3.97 (t, J = 6.6 Hz, 4H, $OCH_2CH_2CH_2(CH_2)_2CH_3$), 6.95 (s, 1H, Ar*H*).

Synthesis of S5[11]

S1 (4.57 g, 9.67 mmol, 1.00 eq.) and **S4** (4.74 g, 14.51 mmol, 1.50 eq.) were added into a 500 mL Schlenk flask, followed by degassing, and the mixture was kept under N_2. Next, THF (60 mL) and triethylamine (30 mL) were added via a gastight syringe. The mixture was degassed with two freeze-pump-thaw cycles, backfilled with N_2. $[Pd(PPh_3)_2Cl_2]$ (135.9 mg, 0.19 mmol, 0.02 eq.) and CuI (18.4 mg, 0.10 mmol, 0.01 eq.) were added under N_2, followed by one freeze-pump-thaw cycle, backfilled with N_2 (320 mL) and H_2 (60 mL). The reaction mixture was stirred at room temperature and monitored by TLC. After the reaction is complete, the mixture was quickly filtered over celite to remove catalyst for avoiding self-coupling of **S5**. The solvent was evaporated *in vacuo* and the crude product was purified by silica column chromatography (DCM:EA = 200:1 to 80:1, v/v) to give **S5** as a yellow solid (5.13 g, 79%).

^{1}H NMR (400 MHz, CD_2Cl_2): δ (ppm): 0.85-0.93 (m, 12H, $OCH_2CH_2CH_2(CH_2)_2CH_3$), 1.30-1.39 (m, 16H, $OCH_2CH_2CH_2(CH_2)_2CH_3$), 1.43-1.54 (m, 8H, $OCH_2CH_2CH_2(CH_2)_2CH_3$), 1.80 (m, 8H, $OCH_2CH_2CH_2(CH_2)_2CH_3$), 2.70 (t, J = 6.1 Hz, 2H, CH_2CH_2OH), 3.38 (s, 1H, alkyne *H*), 3.77 (t, J = 6.1 Hz, 2H, CH_2CH_2OH), 3.98 (m, 8H, $OCH_2CH_2CH_2(CH_2)_2CH_3$), 6.90-6.99 (m, 4H, Ar*H*).

Synthesis of S7

S5 (1.52 g, 2.27 mmol, 1.00 eq.) and **S2** (1.43 g, 2.86 mmol, 1.26 eq.) were added into a 250 mL Schlenk flask, followed by degassing, and the mixture was kept under N_2. Next, THF (30 mL) and triethylamine (10 mL) were added via a gastight syringe. The mixture was degassed with two freeze-pump-thaw cycles, backfilled with N_2. Then, $[Pd(PPh_3)_2Cl_2]$ (33.4 mg, 0.05 mmol, 0.02 eq.) and CuI (4.5 mg, 0.02 mmol, 0.01 eq.) were added under N_2, followed by one freeze-pump-thaw cycle, backfilled with N_2. The reaction mixture was stirred at room temperature overnight, and then was diluted with DCM and filtered over celite. The solvent was evaporated *in vacuo* and the crude product **S6** was dissolved in the mixed solvent of THF (40 mL) and MeOH (0.8 mL), followed by adding TBAF (2.0 mL, 1.0 M in THF) at 0°C. After the reaction mixture was stirred at room temperature for 0.5 h, the solution was diluted with saturated NH_4Cl solution (40 mL) and extracted with DCM (3×40 mL), and the combined extract was dried over Na_2SO_4 and filtered. The solvent was removed *in vacuo* and the crude product was purified by silica column chromatography (DCM:EA = 100:1, v/v) to give **S7** as a light-yellow solid (1.60 g, 73%).

^{1}H NMR (400 MHz, CD_2Cl_2): δ (ppm): 0.83-0.93 (m, 18H, $OCH_2CH_2CH_2(CH_2)_2CH_3$), 1.29-1.40 (m, 24H, $OCH_2CH_2CH_2(CH_2)_2CH_3$), 1.44-1.53 (m, 12H, $OCH_2CH_2CH_2(CH_2)_2CH_3$), 1.75-1.89 (m, 12H, $OCH_2CH_2CH_2(CH_2)_2CH_3$), 2.71 (t, J = 6.1 Hz, 2H, CH_2CH_2OH), 3.38 (s, 1H, alkyne *H*), 3.78 (t, J = 6.1 Hz, 2H, CH_2CH_2OH), 3.94-4.07 (m, 12H, $OCH_2CH_2CH_2(CH_2)_2CH_3$), 6.90-7.03 (m, 6H, Ar*H*).

Synthesis of 4-BBT-OPE$_3$-OH (S8)

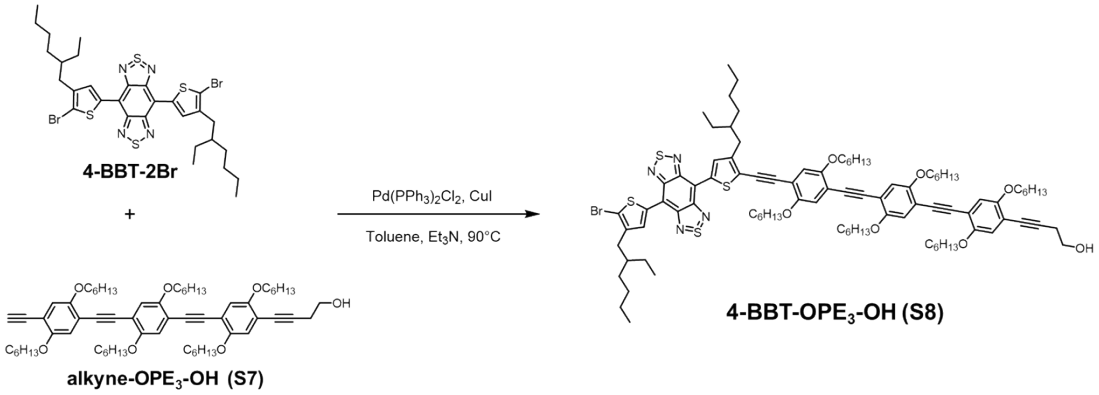

Scheme S2. Synthesis of 4-BBT-OPE$_3$-OH.

4-BBT-2Br (200.7 mg, 0.27 mmol, 1.00 eq.) and **S7** (263.6 mg, 0.27 mmol, 1.00 eq.) were added into a 250 mL Schlenk flask, followed by degassing, and the mixture was kept under N_2. Next, toluene (30 mL) and triethylamine (10 mL) were added via a gastight syringe. The mixture was degassed with two freeze-pump-thaw cycles, backfilled with N_2. [$Pd(PPh_3)_2Cl_2$] (5.7 mg, 8.13×10^{-3} mmol, 0.03 eq.) and CuI (1.6 mg, 8.13×10^{-3} mmol, 0.03 eq.) were added under N_2, followed by one freeze-pump-thaw cycle, backfilled with N_2. The reaction mixture was stirred at 90°C for 6 h and monitored by TLC, and it was diluted with DCM and filtered over celite. The solvent was then removed *in vacuo* and the crude product was purified by silica column

chromatography (DCM:EA = 50:1 to 20:1, v/v) to give 4-BBT-OPE$_3$-OH (**S8**) as a blackish green solid (132.2 mg, 30%).

^{1}H NMR (500 MHz, CD_2Cl_2): δ (ppm): 0.80-1.04 (m, 30H), 1.17-1.53 (m, 52H), 1.74-1.97 (m, 14H), 2.66 (d, J = 7.1 Hz, 2H), 2.71 (t, J = 6.1 Hz, 2H), 2.87 (d, J = 7.0 Hz, 2H), 3.78 (m, 2H), 3.94-4.10 (m, 12H), 6.92-7.05 (m, 6H). 8.66 (s, 1H). 8.84 (s, 1H). HRMS (MALDI-TOF): calculated for $[M]^+$: 1630.7615; found: 1630.7594. GPC: M_n^{GPC} = 2100 g/mol, $Đ = M_w/M_n$ = 1.01.

Synthesis of 4-BBT-OPE$_3$-alkyne (S9)

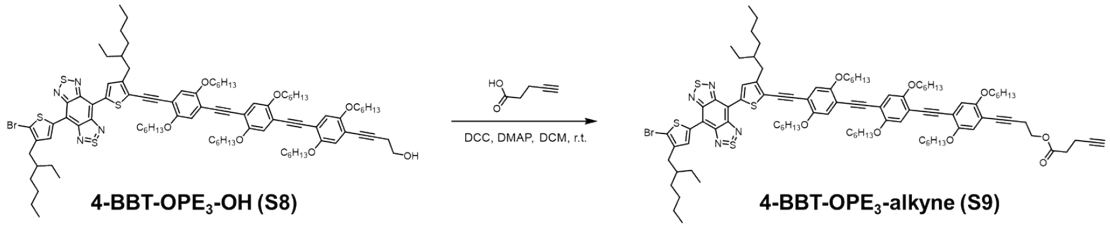

Scheme S3. Synthesis of 4-BBT-OPE$_3$-alkyne.

S8 (50.0 mg, 0.03 mmol, 1.00 eq.), 4-pentynoic acid (15.2 mg, 0.15 mmol, 5.00 eq.), DCC (32.0 mg, 0.15 mmol, 5.00 eq.) and DMAP (1.1 mg, 0.01 mmol, 0.30 eq.) were added into a 50 mL Schlenk flask, followed by degassing, and the mixture was kept under N_2. Next, DCM (5 mL) was added via a gastight syringe. After the reaction mixture was stirred at room temperature overnight, the solvent was removed *in vacuo* and the crude product was purified by silica column chromatography (DCM:hexane = 2:1, v/v) to give alkyne-terminated 4-BBT-OPE$_3$-alkyne (**S9**) as a blackish green solid (45.1 mg, 88%). The product was subjected to ^{1}H NMR (Figures 1a and S10) and GPC analysis (Figure S9, Table S1), and its "absolute" molecular weight was determined by

MALDI-TOF-MS (Figure S12).

^{1}H NMR (500 MHz, CD_2Cl_2): δ (ppm): 0.82-1.04 (m, 30H), 1.19-1.63 (m, 52H), 1.76-1.95 (m, 14H), 2.01 (t, ^4J = 2.5 Hz, 1H), 2.51 (td, ^3J = 7.1 Hz, ^4J = 2.3 Hz, 2H), 2.59 (t, ^3J = 7.1 Hz, 2H), 2.66 (d, J = 7.2 Hz, 2H), 2.82 (t, J = 6.9 Hz, 2H), 2.88 (d, J = 7.1 Hz, 2H), 3.92-4.10 (m, 12H), 4.29 (t, J = 7.1 Hz, 2H), 6.92-7.05 (m, 6H). 8.72 (s, 1H). 8.90 (s, 1H). HRMS (MALDI-TOF): calculated for $[M]^+$: 1710.7879; found: 1710.7838. GPC: M_n^{GPC} = 1700 g/mol, $Đ = M_w/M_n$ = 1.01.

Synthesis of N_3-CTA

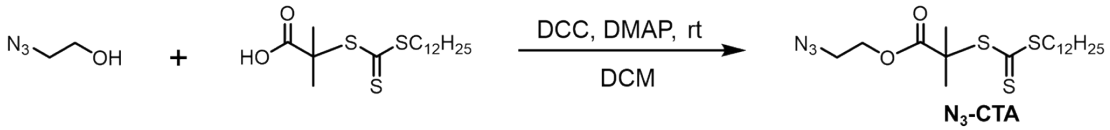

Scheme S4. Synthesis of N_3-CTA.

2-(Dodecylthiocarbonothioylthio)-2-methylpropionic acid (4.03 g, 11.05 mmol, 1.06 eq.), DCC (3.23 g, 15.65 mmol, 1.50 eq.) and DMAP (0.13 g, 1.06 mmol, 0.10 eq.) were dissolved in 50 mL of dry CH_2Cl_2. The solution was cooled to 0°C with an ice bath. Subsequently, 2-azidoethan-1-ol (0.91 g, 0.80 mL, 10.45 mmol, 1.00 eq.) was added dropwise and the final solution was left to stir overnight at room temperature. The mixture was filtered to remove the side product of DCU and the filtrate was washed with water and dried over Na_2SO_4. After the evaporation of solvent, the crude product was purified by silica column chromatography (hexane:DCM = 1:1, v/v), yielding N_3-CTA (3.40 g, 75%) as an orange-yellow oil.

^{1}H NMR (400 MHz, $CDCl_3$): δ (ppm): 0.88 (t, J = 7.1 Hz, 3H, CH_2CH_3), 1.22-1.43

(m, 18H, $CS_3CH_2CH_2(CH_2)_9CH_3$), 1.66 (m, 2H, $CS_3CH_2CH_2(CH_2)_9CH_3$), 1.71 (s, 6H, $CS_3C(CH_3)_2$), 3.27 (t, J = 7.4 Hz, 2H, CS_3CH_2), 3.46 (t, J = 5.1 Hz, 2H, $N_3CH_2CH_2$), 4.27 (t, J = 5.1 Hz, 2H, $N_3CH_2CH_2$).

Synthesis of N_3-P2VP

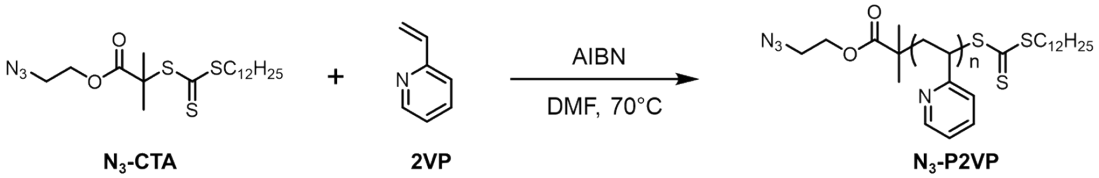

Scheme S5. Synthesis of N_3-P2VP.

The feed ratio of chain transfer agent (N_3-CTA) to monomer (2VP) was set as 1:40. Solution RAFT homopolymerization of 2VP was performed in DMF at 70°C using the as-prepared azide-terminated chain transfer agent. 2VP (3.00 g, 3.08 mL, 28.53 mmol), N_3-CTA (0.31 g, 0.71 mmol) and AIBN (0.04 g, 0.24 mmol) were introduced into a 25 mL Schlenk flask sealed with a rubber septum for degassing, and the mixture was kept under N_2. Next, dry DMF (8 mL) was charged via a gastight syringe. The flask was degassed by three freeze-pump-thaw cycles followed by immersing the flask into an oil bath set at 70°C. The polymerization lasted 8 h and was then terminated by putting the flask into liquid N_2. The reaction mixture was precipitated into cold diethyl ether. The crude product was purified by precipitation in cold hexane three times followed by drying *in vacuo* overnight to give 1.26 g (38%) of light yellow solid, N_3-P2VP, which was subjected to GPC (Figure S15 and Table S1) and ^{1}H NMR (Figure S14) analysis. Its 'absolute' molecular weight was determined by ^{1}H NMR after coupling.

GPC: M_n ^{GPC} = 2900 g/mol, $Đ = M_w/M_n$ = 1.11.

Synthesis of 4-BBT-OPE$_3$-*b*-P2VP$_{22}$ (S10)

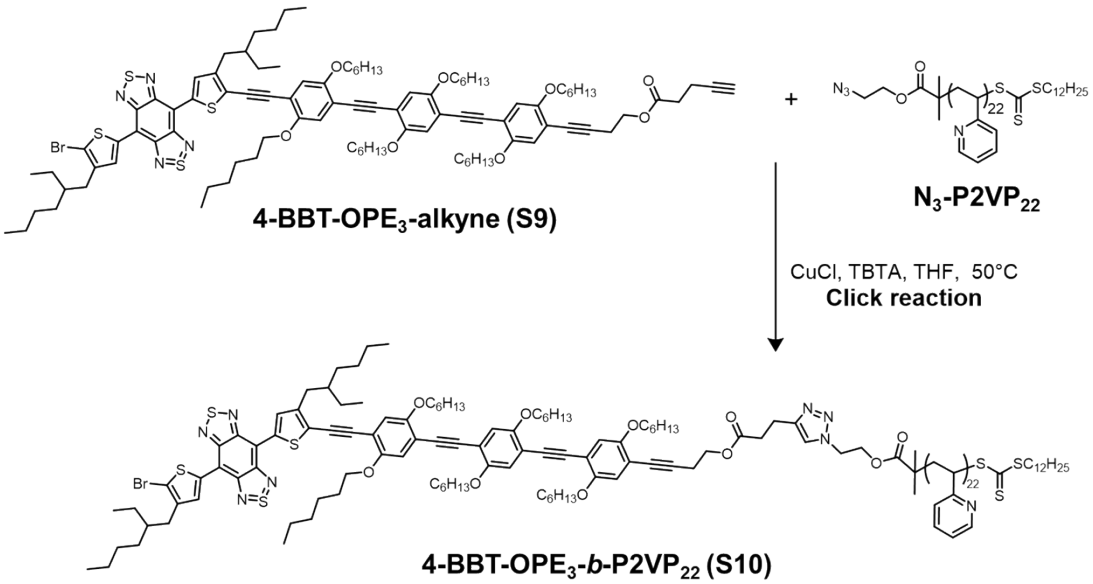

Scheme S6. Synthesis of 4-BBT-OPE$_3$-*b*-P2VP$_{22}$.

Cu-catalyzed-alkyne-azide-cycloaddition (CuAAC) reaction was used to synthesize 4-BBT-OPE$_3$-*b*-P2VP$_{22}$ diblock copolymer between alkyne-terminated 4-BBT-OPE$_3$-alkyne (**S9**) and N$_3$-P2VP. **S9** (23.0 mg, 13.44 μmol, 1.00 eq.), N$_3$-P2VP (50.0 mg, 17.24 μmol, 1.30 eq.), CuCl (21.4 mg, 40.32 μmol, 3.00 eq.) and TBTA (4.0 mg, 40.32 mmol, 3.00 eq.) were added into a 25 mL Schlenk flask followed by degassing, and the mixture was kept under N$_2$. Next, THF (6 mL) was added via a gastight syringe. The mixture was degassed with three freeze-pump-thaw cycles, backfilled with N$_2$, and then the reaction mixture was stirred at 50°C for 24 h. The solvent was evaporated and the residue was purified by silica column chromatography (DCM:MeOH:TEA = 10:1:2, v/v/v) to remove the unreacted alkyne-terminated 4-BBT-OPE$_3$-alkyne and CuCl. To remove excess N$_3$-P2VP, the crude product was purified by repeated precipitation in acetonitrile (v/v = 1/10) three times, followed by drying *in vacuo* overnight to give 4-BBT-OPE$_3$-*b*-P2VP$_{22}$ (**S10**) diblock copolymer as a blackish green solid (48.4 mg,

81%). This diblock copolymer was subjected to GPC analysis (Figure S17, Table S1), and the number average degree of polymerization of P2VP block (DP_n = 22) was determined by ^{1}H NMR on the basis of known DP_n of 4-BBT-OPE$_3$ (Figure S16).

GPC: M_n^{GPC} = 5300 g/mol, $Đ = M_w/M_n$ = 1.08.

Additional results and discussion

Given excellent crystallinity of OPE segments and NIR photothermal activity of BBT unit, alkyne-terminated 4-BBT-OPE_3 was synthesized by iterative Sonogashira coupling reaction (Schemes 1c and S1-3). Characteristic peaks "a,b", "c", "f" "g", "g′" and "o" appeared at 6.92-7.05, 3.92-4.11, 0.85-1.01, 8.72, 8.90 and 4.29 ppm, respectively in ^{1}H nuclear magnetic resonance (NMR) spectrum of alkyne-terminated 4-BBT-OPE_3 (Figure S17a). A predominant m/z peak at 1710.7838 appeared in matrix-assisted laser desorption/ionization time-of-flight (MALDI-TOF) mass spectrum of alkyne-terminated 4-BBT-OPE_3 (Figure S17c), consistent with the theoretic value (1710.7879). The isotope pattern of expanded spectrum is also in agreement with the theoretic prediction (Figure S17c). Subsequently, alkyne-terminated 4-BBT-OPE_3 was connected with azide-terminated P2VP by Cu-catalyzed alkyne-azide cycloaddition reaction to give 4-BBT-OPE_3-*b*-$P2VP_{22}$ (Schemes 1c and S6, Figures S16, S17b, and S17d). Gel permeation chromatography (GPC) analysis of purified product showed a unimodal peak with a molecular weight distribution of 1.08 and much short retention time than those of alkyne-terminated 4-BBT-OPE_3 and azide-terminated P2VP, indicative of successful synthesis of 4-BBT-OPE_3-*b*-$P2VP_{22}$ and complete removal of unreacted 4-BBT-OPE_3 and $P2VP_{22}$ segments (Figure S17d). The number of repeat unit of P2VP segment (N_{2VP}) was estimated to be about 22 on the basis of known molecular weight of 4-BBT-OPE_3 and integral ratio of peaks "w" to "c" ($N_{2VP} = 12*I_w/I_c$) in ^{1}H NMR spectrum of BBT-OPE_3-*b*-$P2VP_{22}$ (Figures S16 and S17b).

Supporting figures

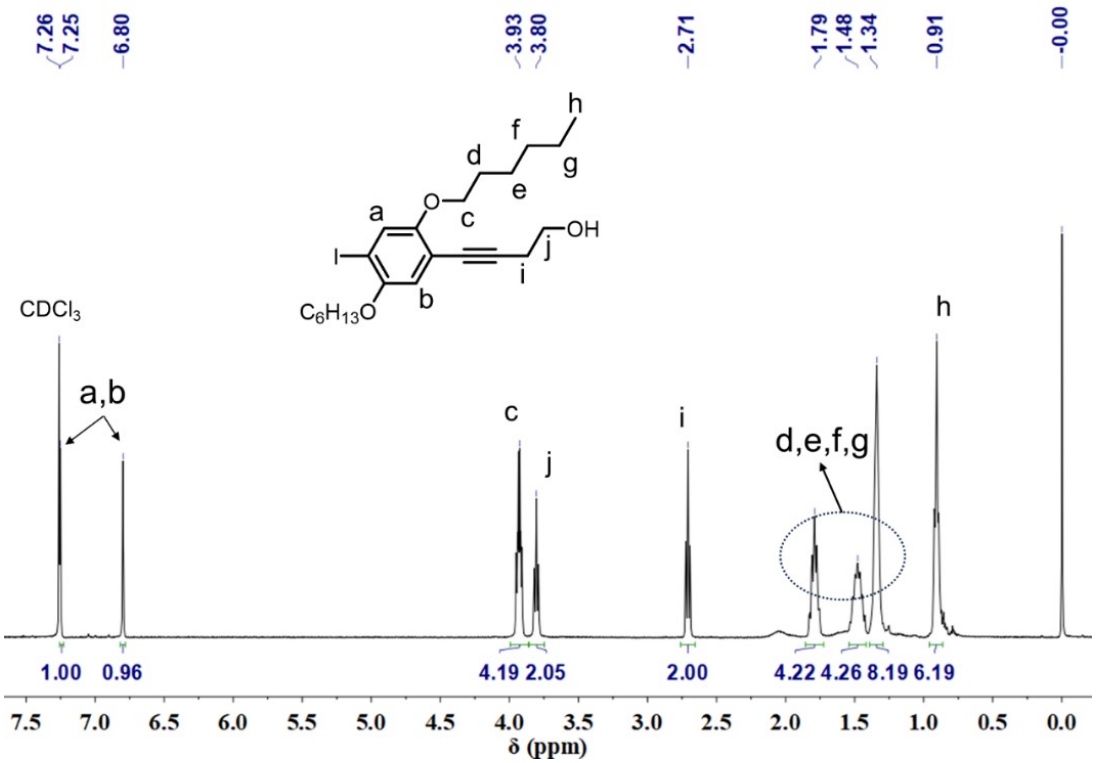

Figure S1. ^{1}H NMR spectrum ($CDCl_3$, 298 K, 400 MHz) of **S1**.

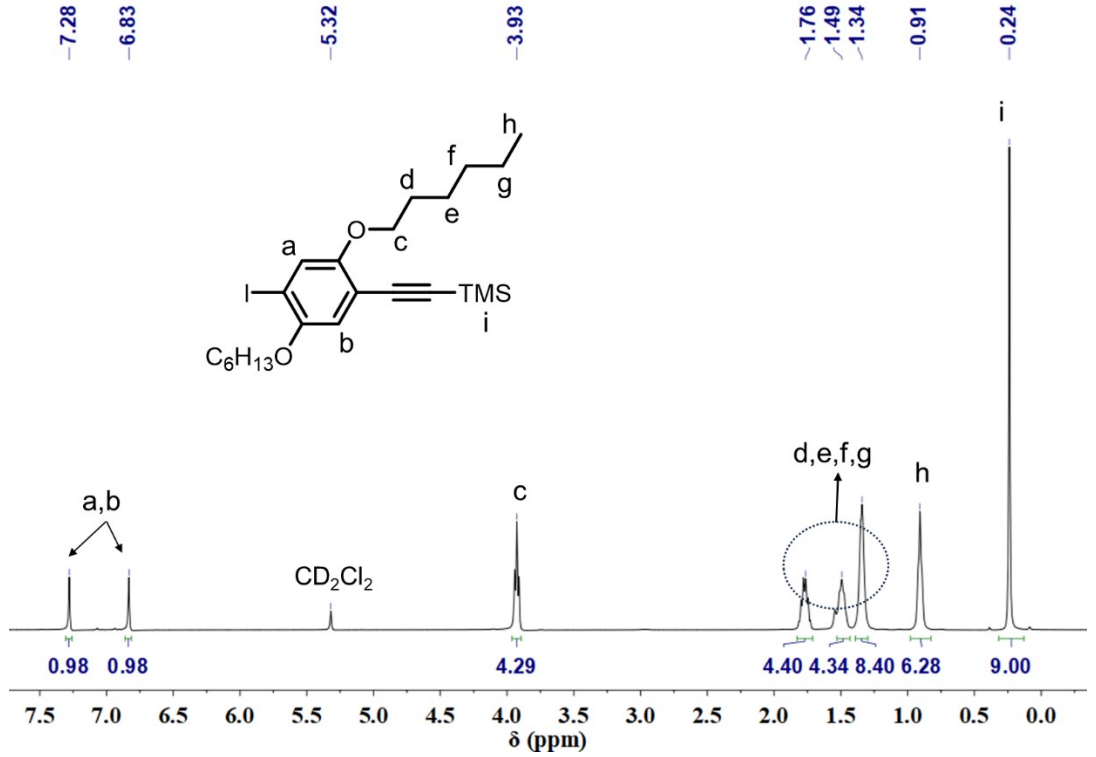

Figure S2. ^{1}H NMR spectrum (CD_2Cl_2, 298 K, 400 MHz) of **S2**.

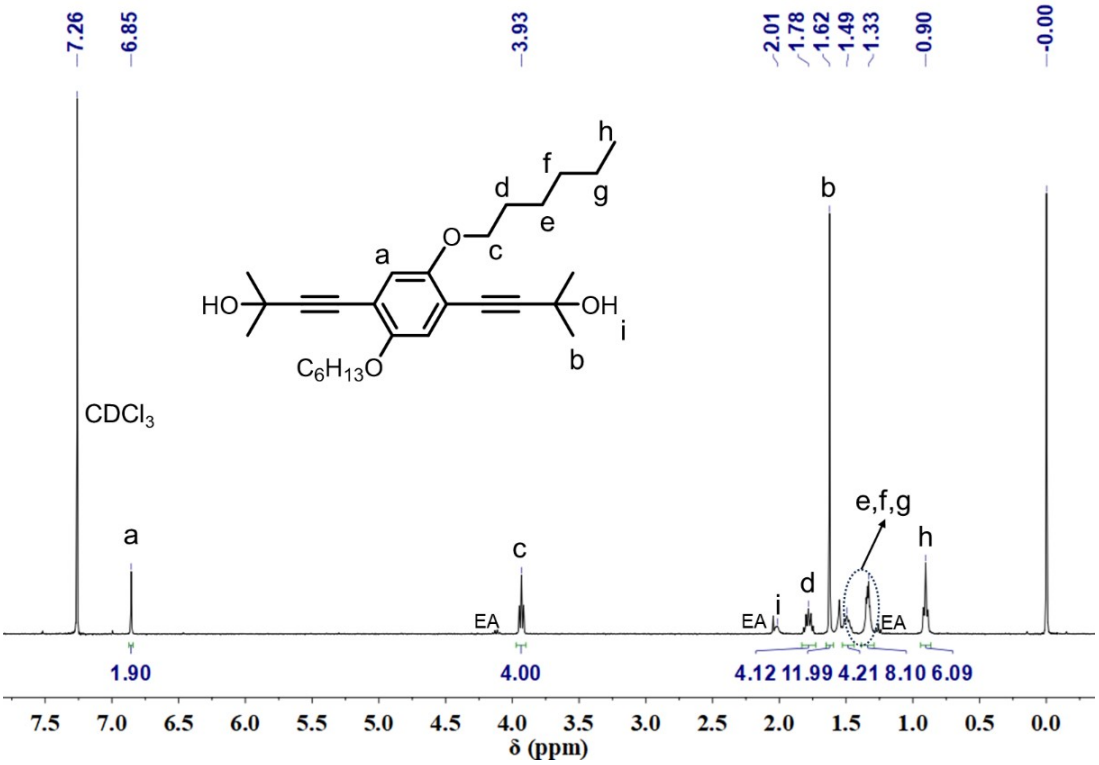

Figure S3. ^{1}H NMR spectrum ($CDCl_3$, 298 K, 400 MHz) of **S3**.

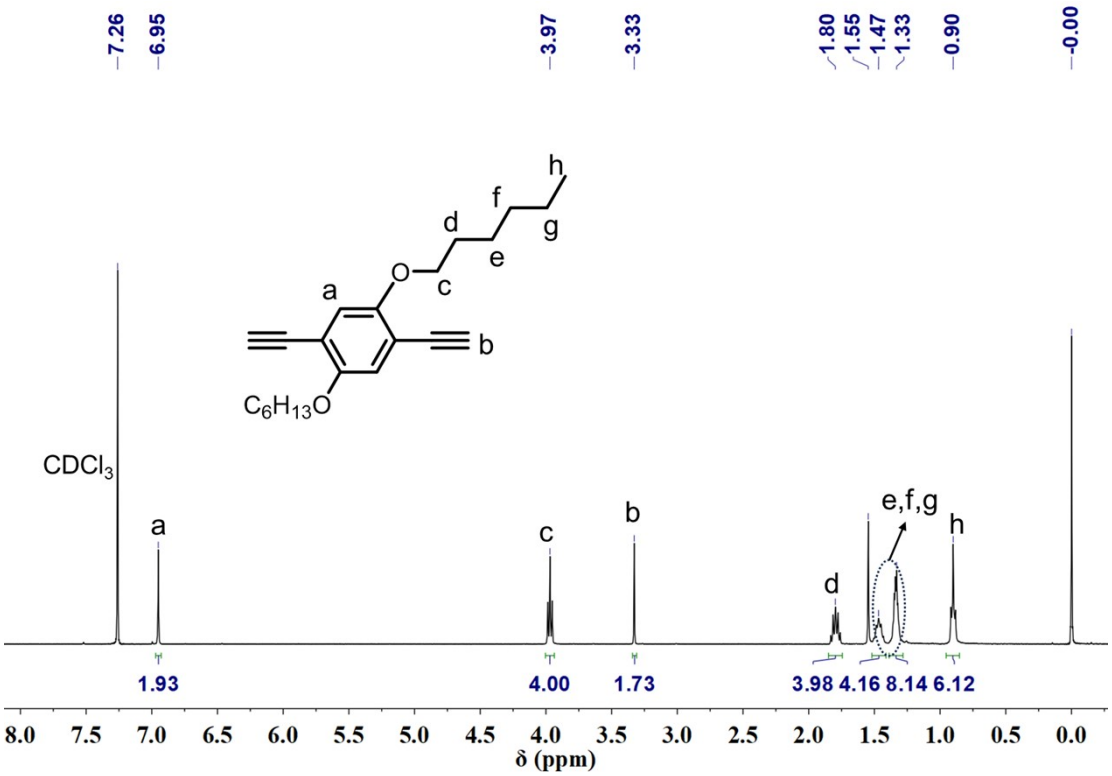

Figure S4. ^{1}H NMR spectrum ($CDCl_3$, 298 K, 400 MHz) of **S4**.

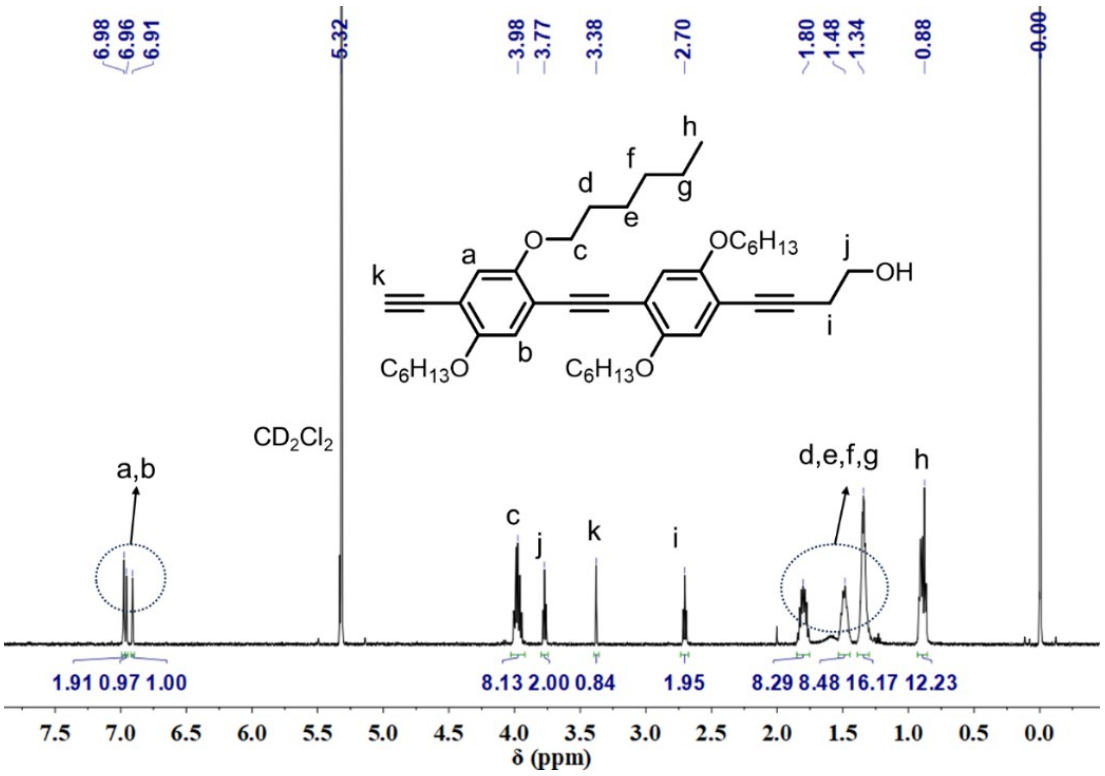

Figure S5. ^{1}H NMR spectrum (CD_2Cl_2, 298 K, 400 MHz) of **S5**.

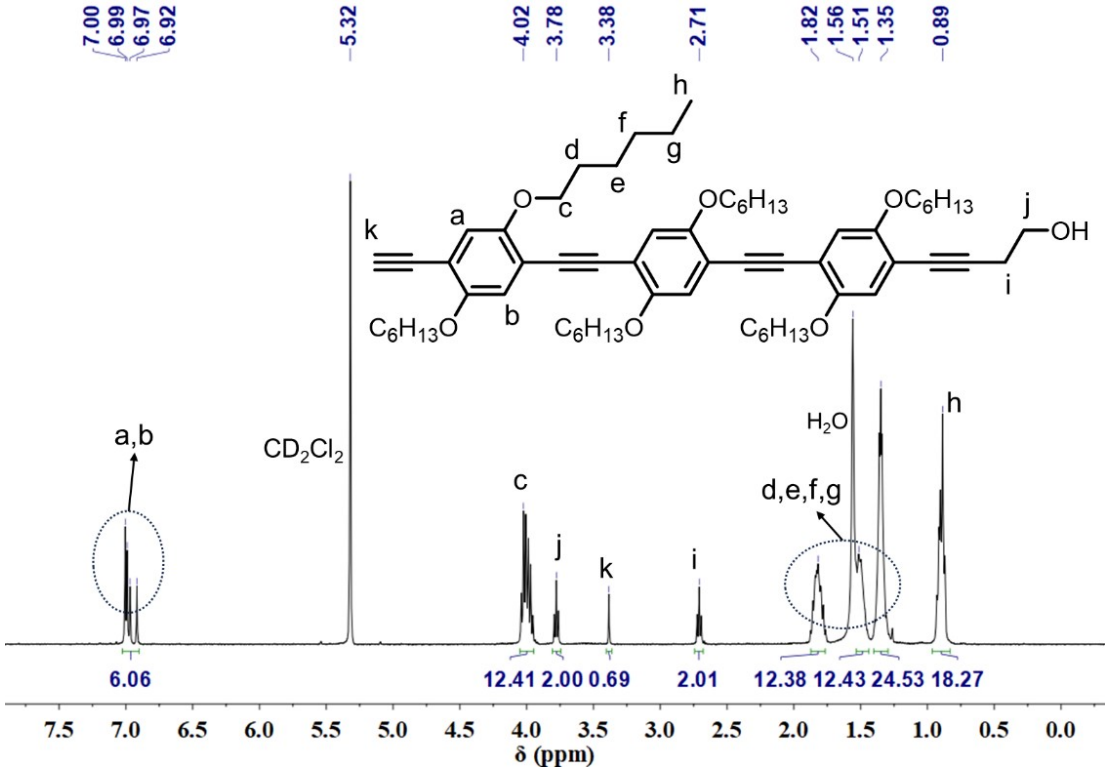

Figure S6. ^{1}H NMR spectrum (CD_2Cl_2, 298 K, 400 MHz) of **S7**.

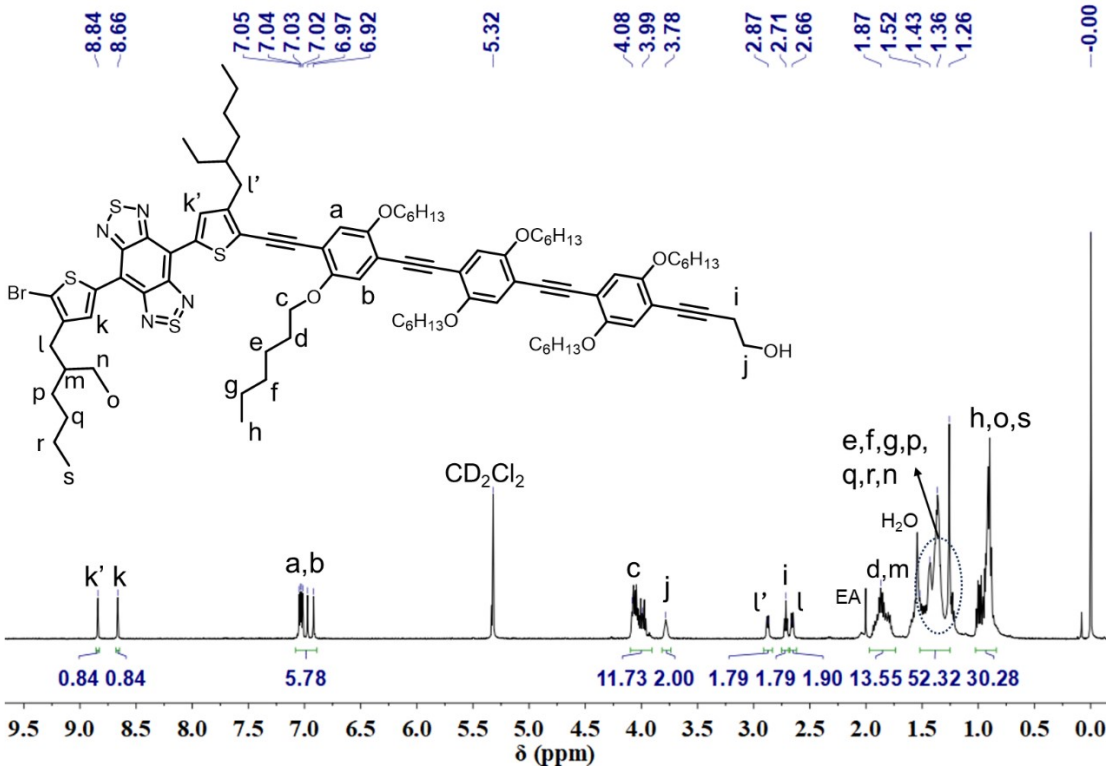

Figure S7. ^{1}H NMR spectrum (CD_2Cl_2, 298 K, 500 MHz) of 4-BBT-OPE$_3$-OH.

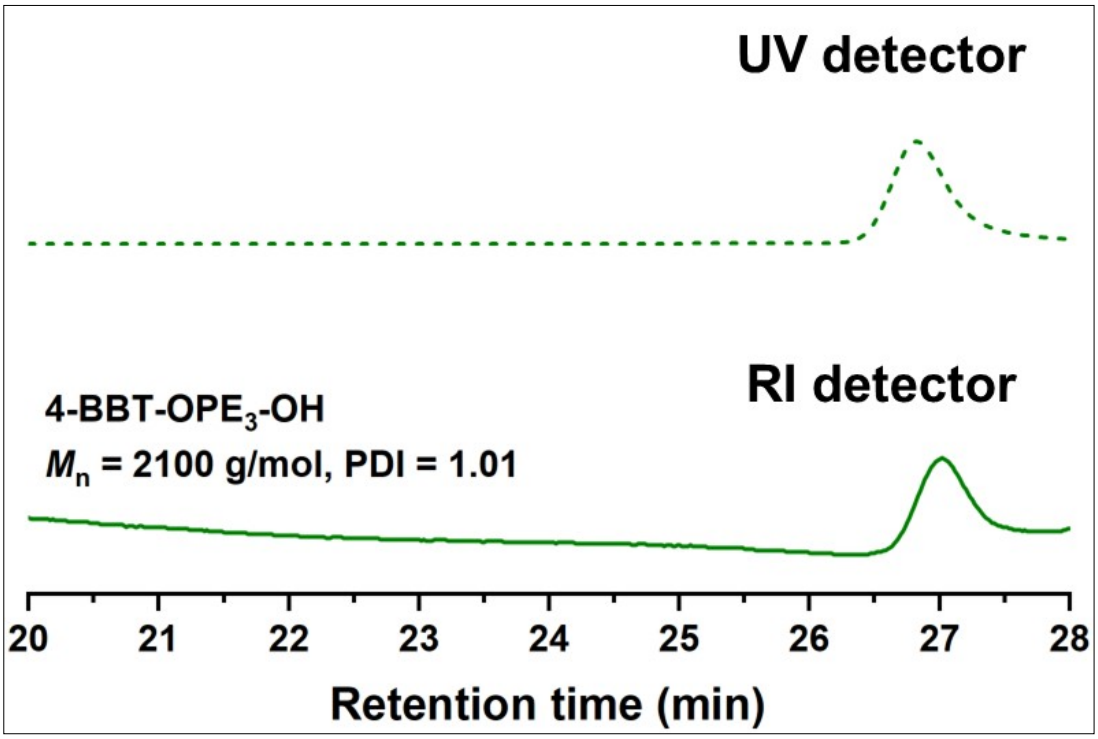

Figure S8. GPC curves of 4-BBT-OPE$_3$-OH.

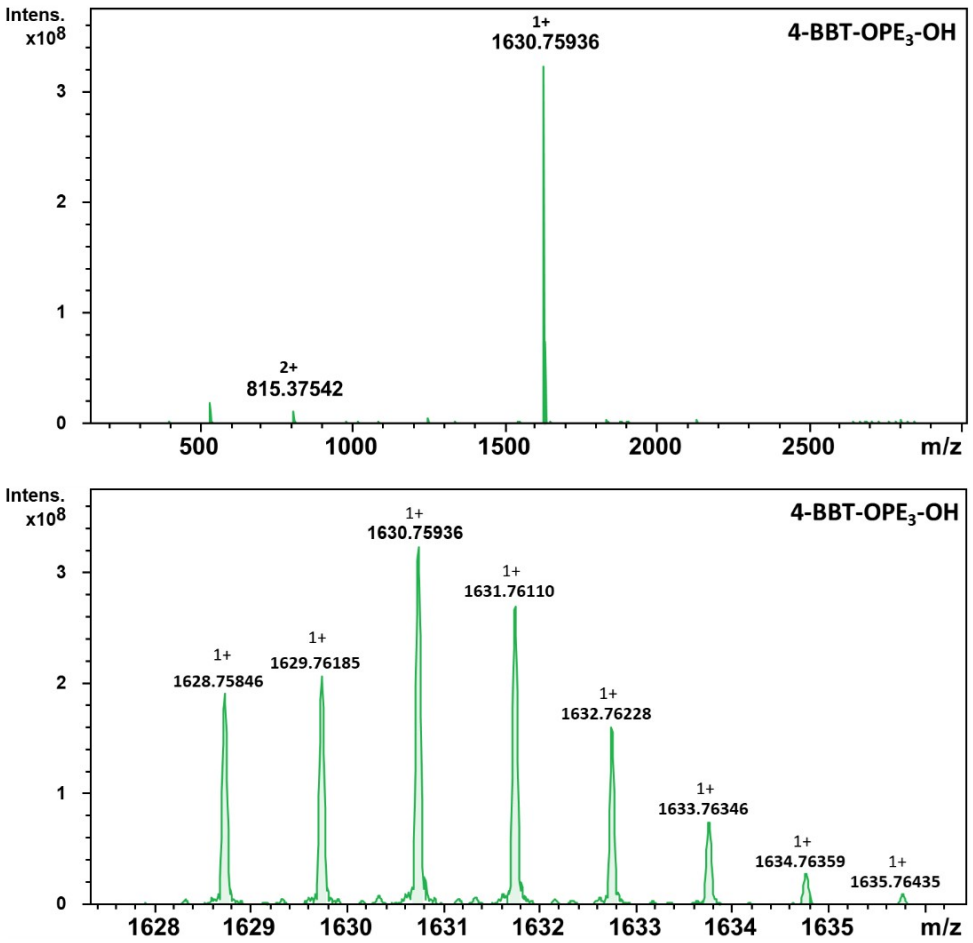

Figure S9. MALDI-TOF-MS spectra of 4-BBT-OPE$_3$-OH.

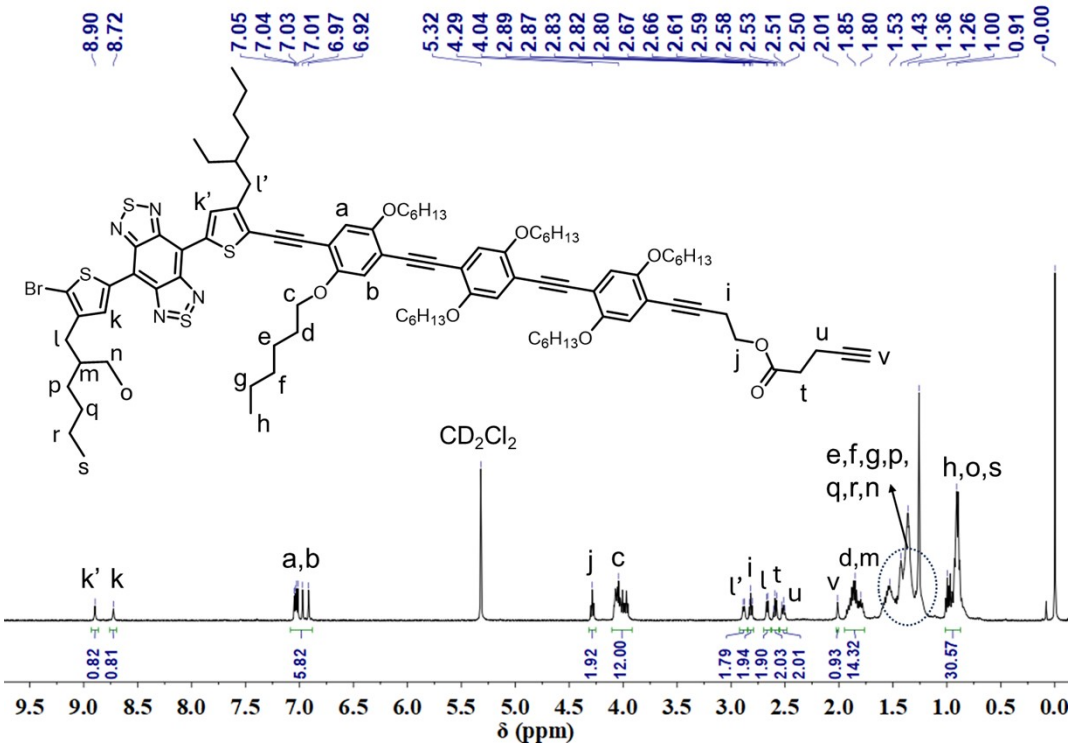

Figure S10. ^{1}H NMR spectrum (CD_2Cl_2, 298 K, 500 MHz) of 4-BBT-OPE$_3$-alkyne.

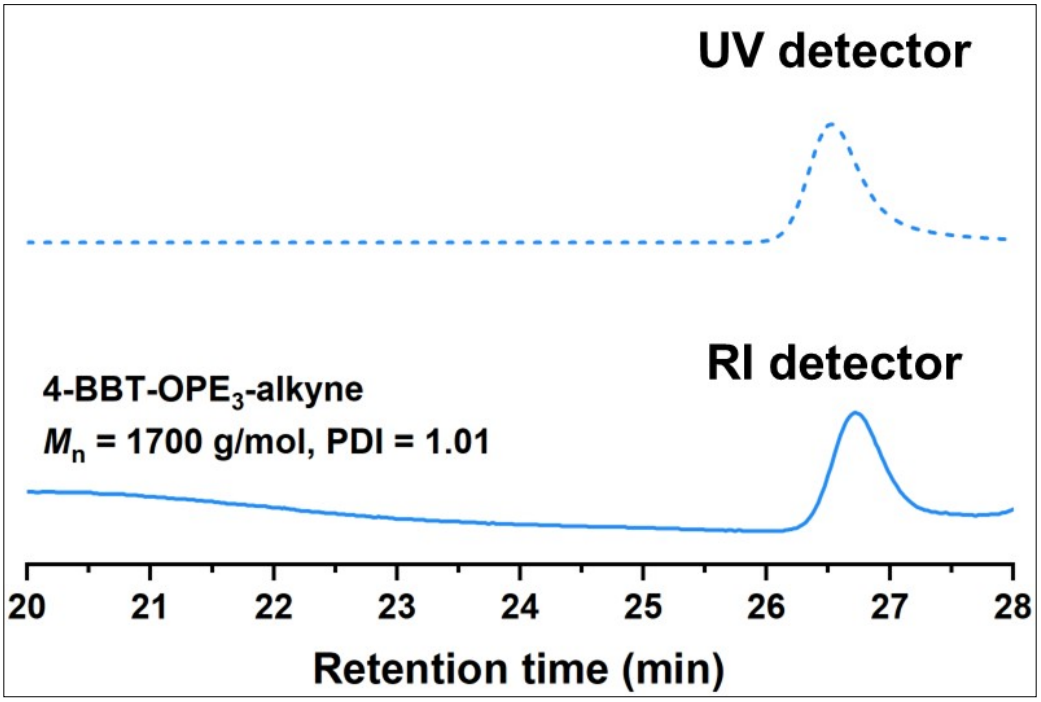

Figure S11. GPC curves of 4-BBT-OPE$_3$-alkyne.

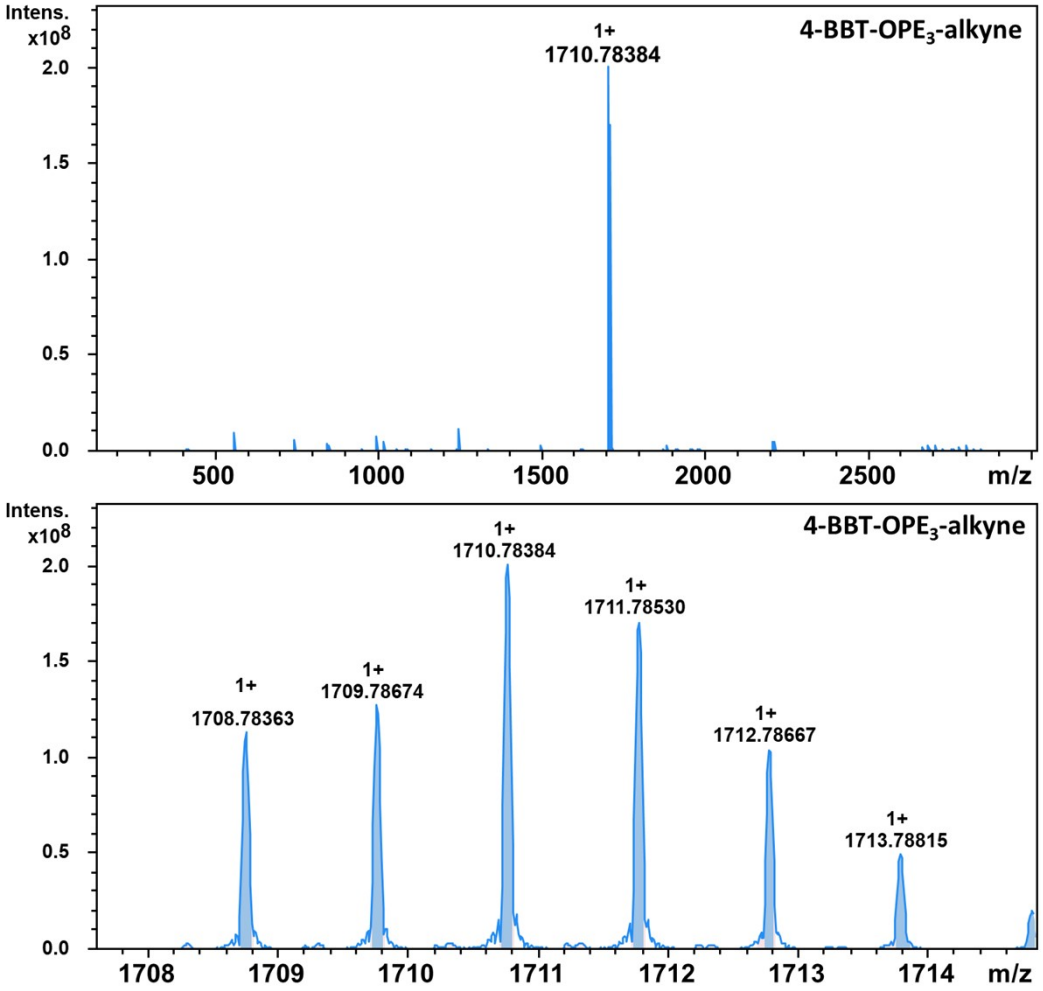

Figure S12. MALDI-TOF-MS spectra of 4-BBT-OPE$_3$-alkyne.

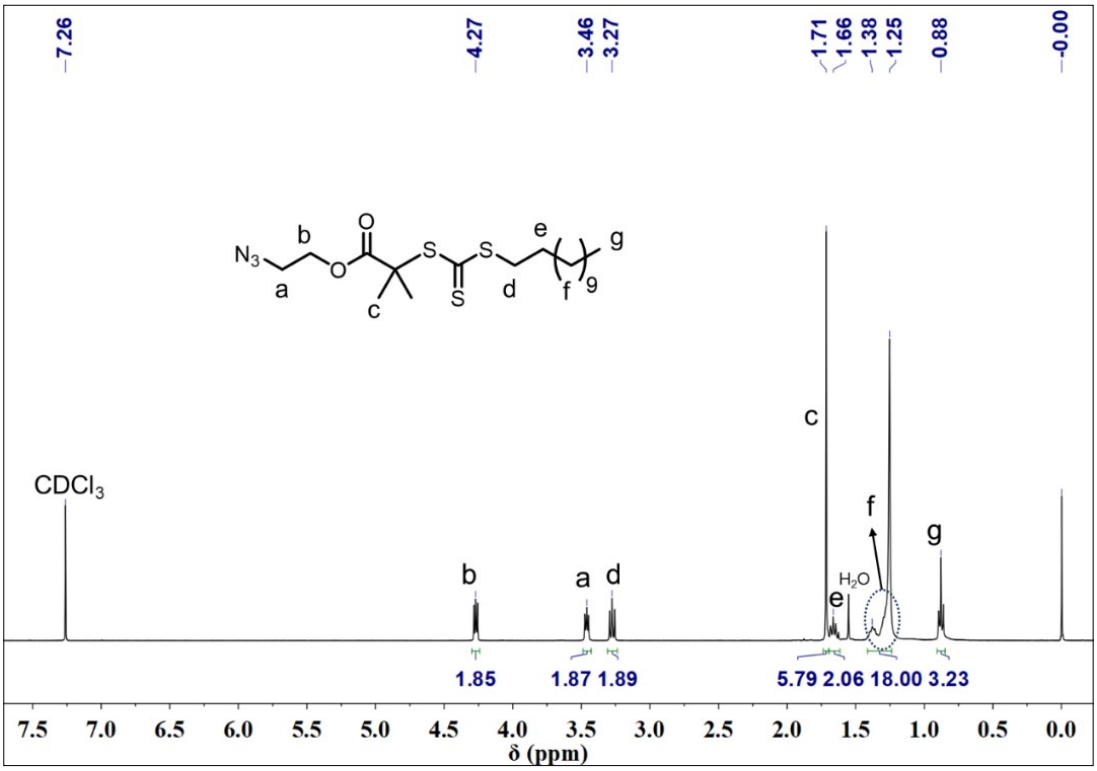

Figure S13. ^{1}H NMR spectrum ($CDCl_3$, 298 K, 400 MHz) of N_3-CTA.

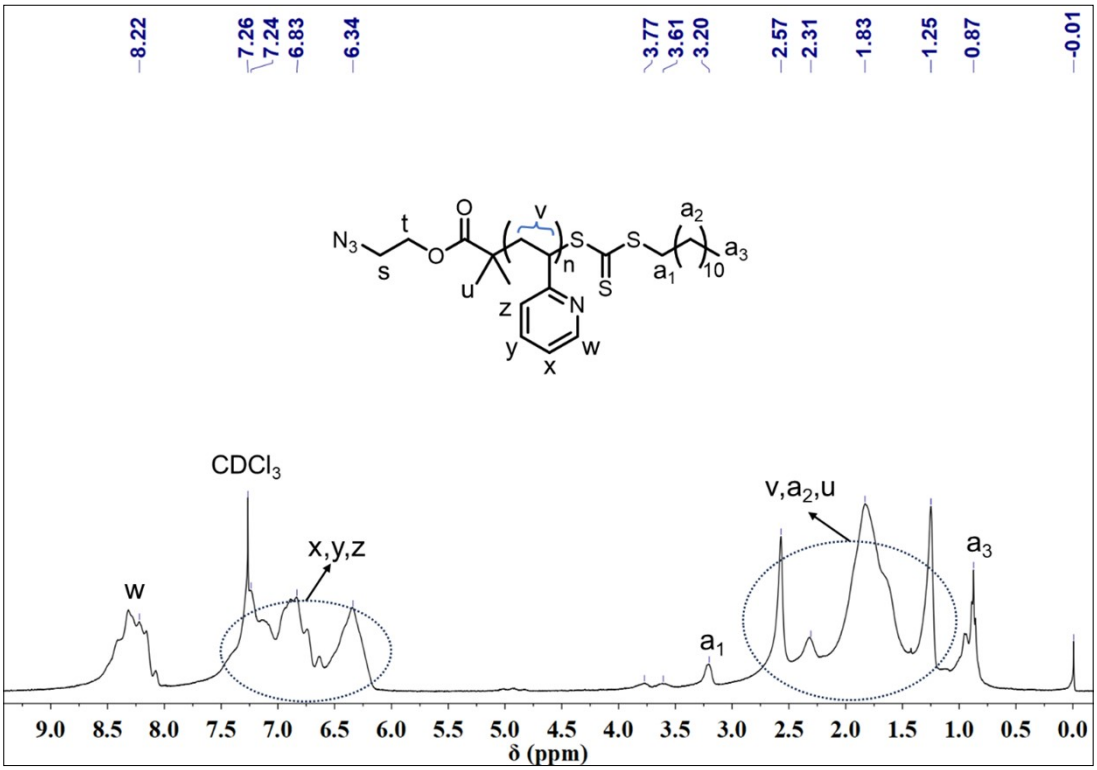

Figure S14. ^{1}H NMR spectrum ($CDCl_3$, 298 K, 400 MHz) of N_3-P2VP.

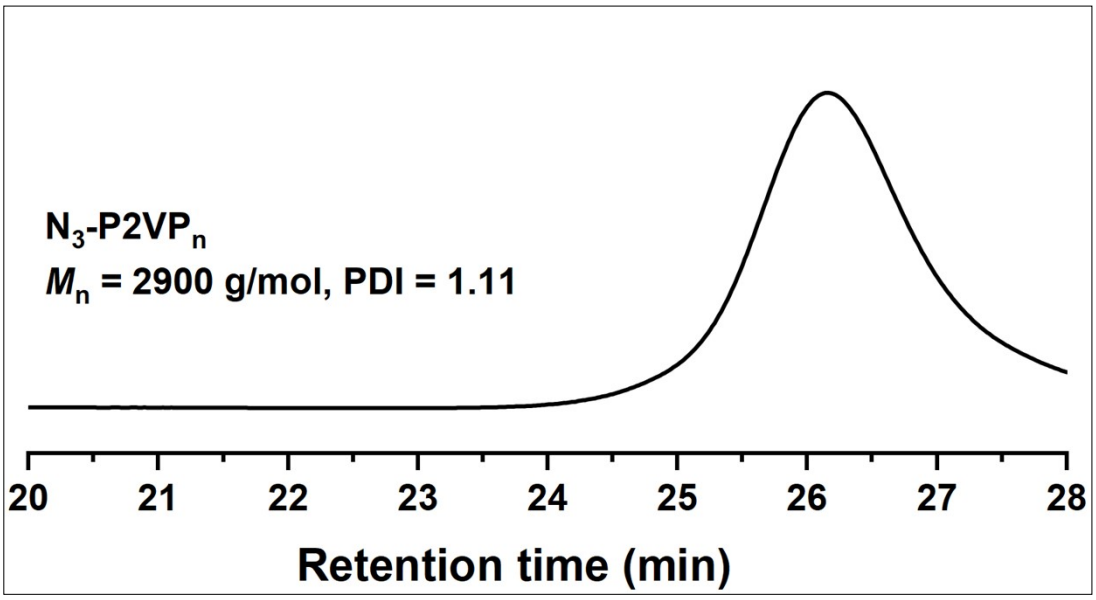

Figure S15. GPC curve of N_3-P2VP.

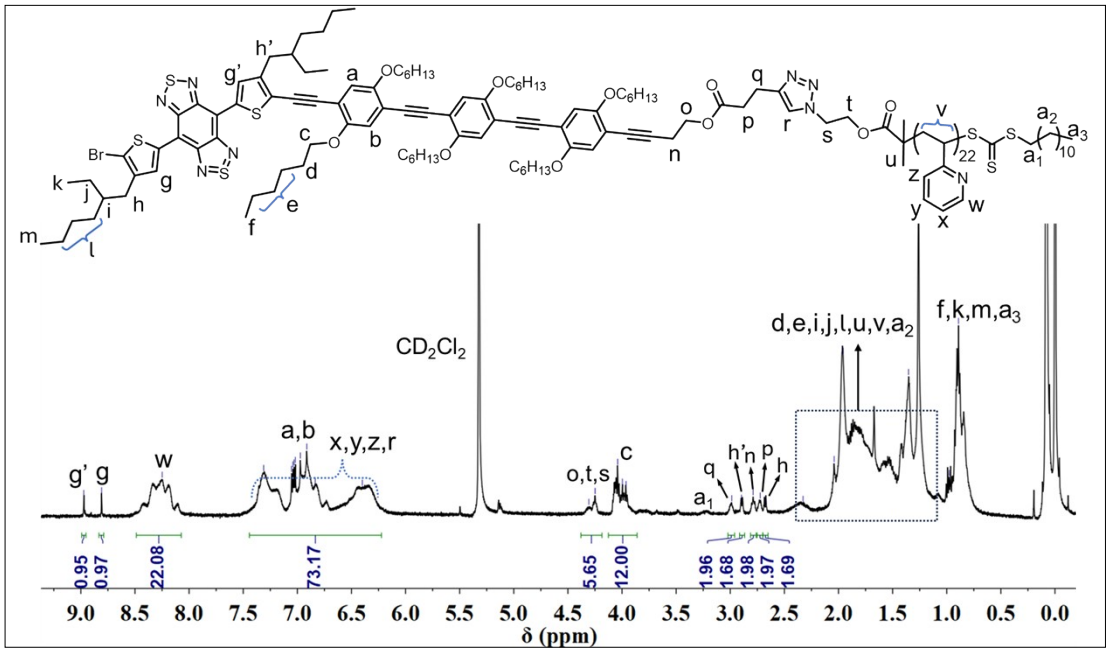

Figure S16. ^{1}H NMR spectrum (CD_2Cl_2, 298 K, 500 MHz) of 4-BBT-OPE$_3$-*b*-P2VP$_{22}$. The number of repeat unit of P2VP segment (N_{2VP}) was estimated to be about 22 on the basis of known molecular weight of 4-BBT-OPE$_3$ and integral ratio of peaks "w" to "c" (N_{2VP} = 12*I_w/I_c = 22).

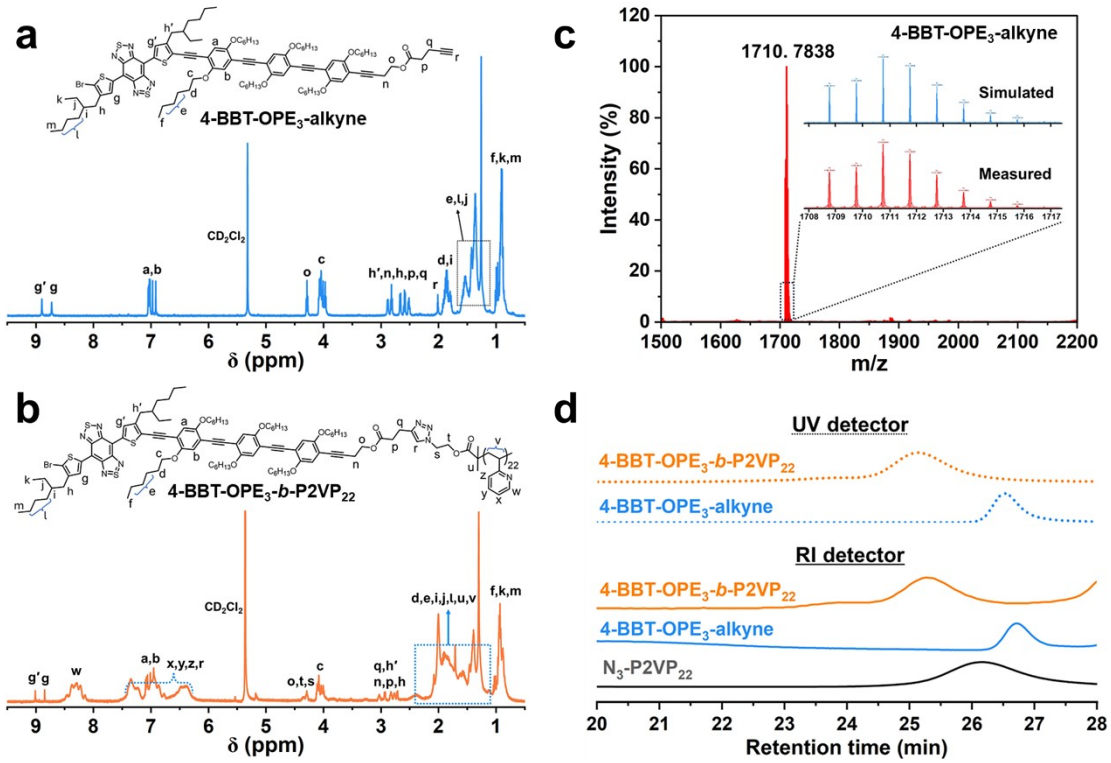

Figure S17. ^{1}H NMR spectra of (a) alkyne-terminated 4-BBT-OPE$_3$ and (b) 4-BBT-OPE$_3$-*b*-P2VP$_{22}$. (c) MALDI-TOF spectrum of alkyne-terminated 4-BBT-OPE$_3$. (d) GPC curves of alkyne-terminated 4-BBT-OPE$_3$, azide-terminated P2VP$_{22}$ and 4-BBT-OPE$_3$-*b*-P2VP$_{22}$.

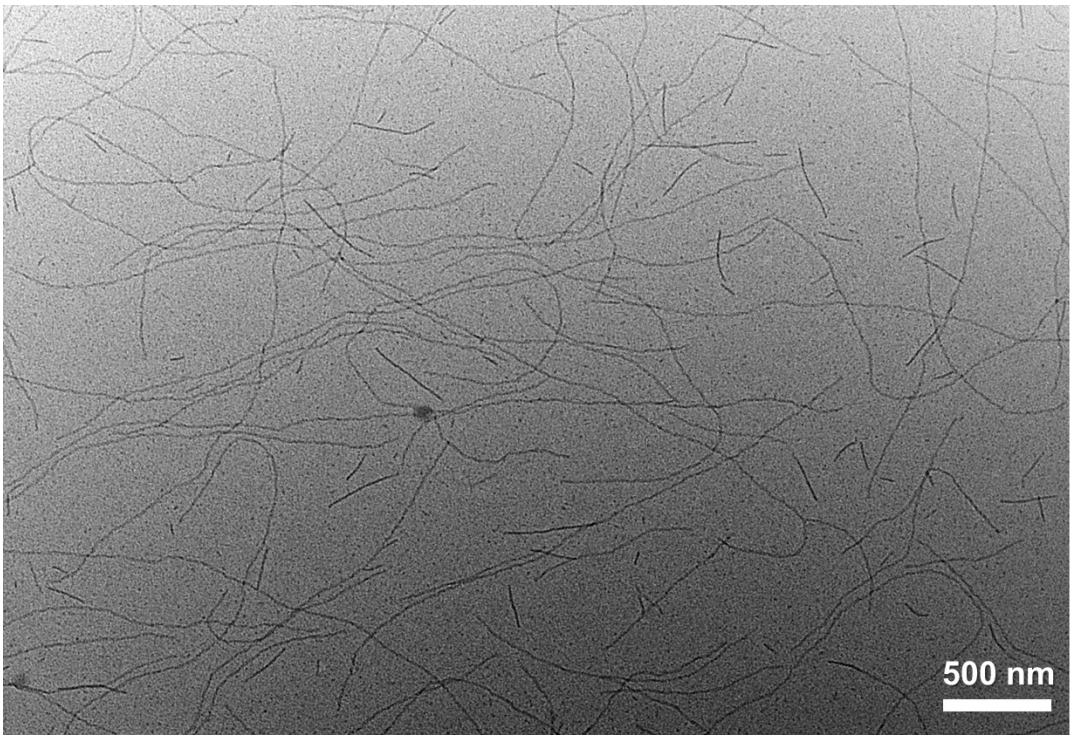

Figure S18. TEM image of micelles of 4-BBT-OPE$_3$-*b*-P2VP$_{22}$ formed by heating/cooling protocol, captured at low magnification.

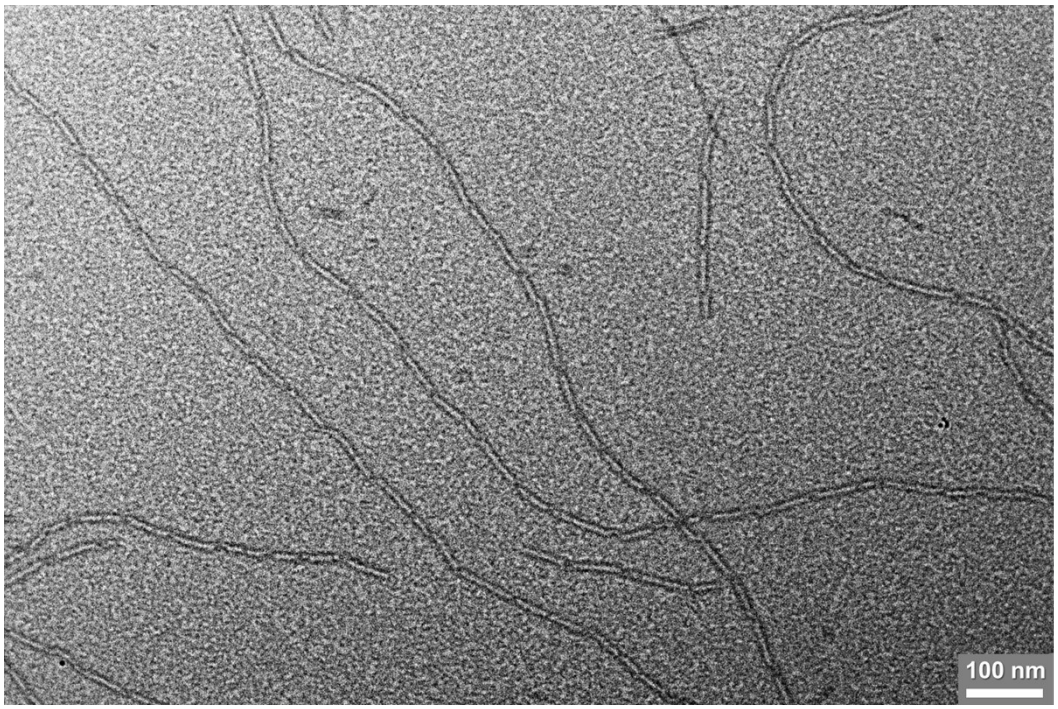

Figure S19. TEM image of micelles of 4-BBT-OPE$_3$-*b*-P2VP$_{22}$ formed by the heating/ cooling protocol, captured at lower magnification. TEM sample was stained with phosphotungstic acid.

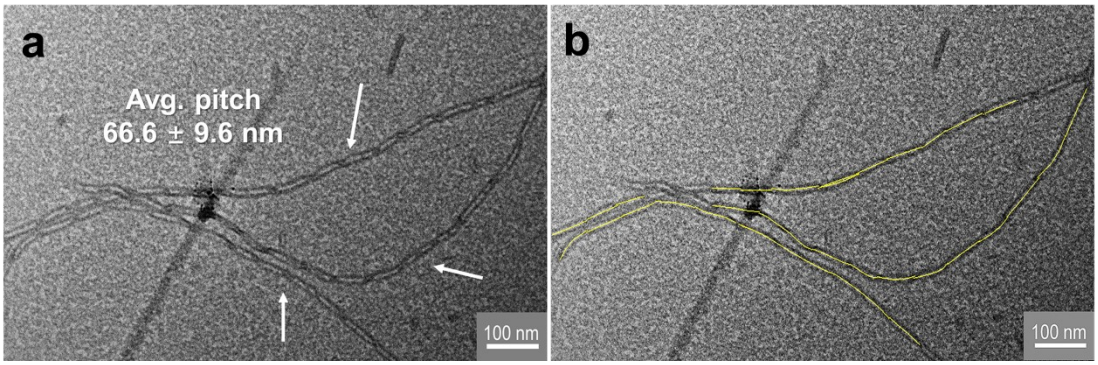

Figure S20. (a) TEM image of helical fiber-like micelles of 4-BBT-OPE$_3$-*b*-P2VP$_{22}$ formed by heating/cooling protocol. TEM sample was stained with phosphotungstic acid. The mean pitch length of micelles was calculated from measurements of over 30 pitches of three helical fiber-like micelles indicated by arrows. (b) TEM image of micelles with markings.

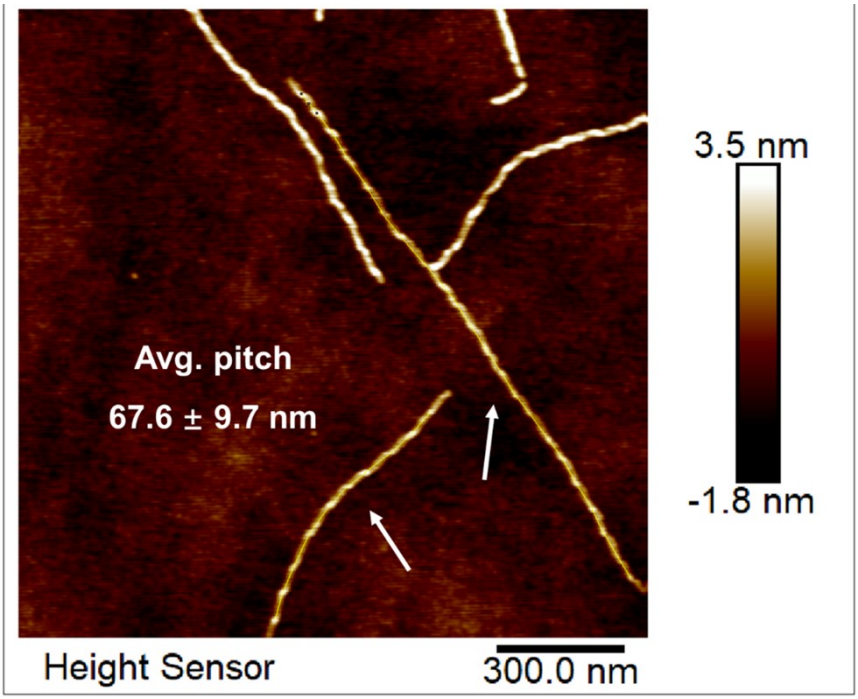

Figure S21. AFM image of helical fiber-like micelles of 4-BBT-OPE$_3$-*b*-P2VP$_{22}$ formed by heating/cooling protocol. The mean pitch length of micelles was calculated from measurements of 30 pitches of two helical fiber-like micelles indicated by arrows.

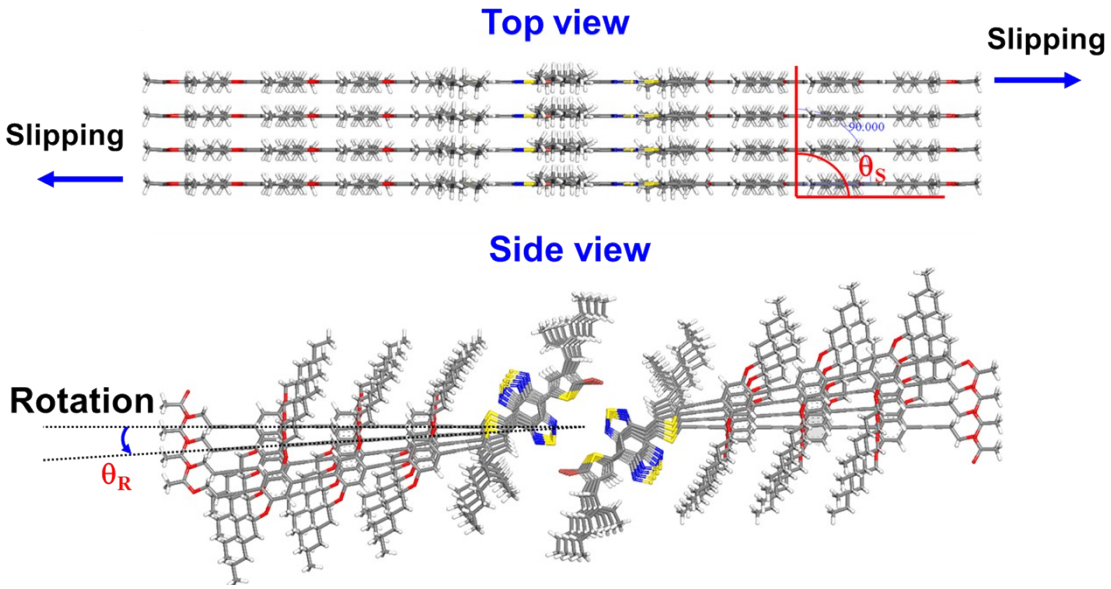

Figure S22. Schematic diagrams of two-column packing mode

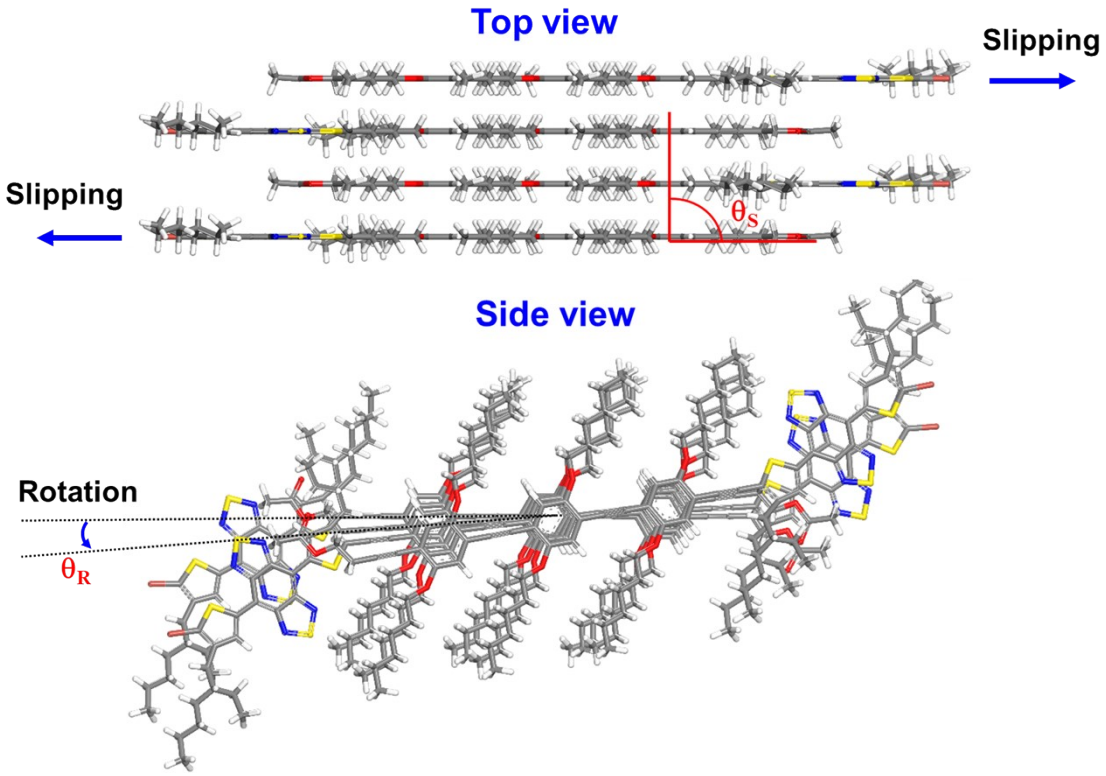

Figure S23. Schematic diagrams of single-column packing mode

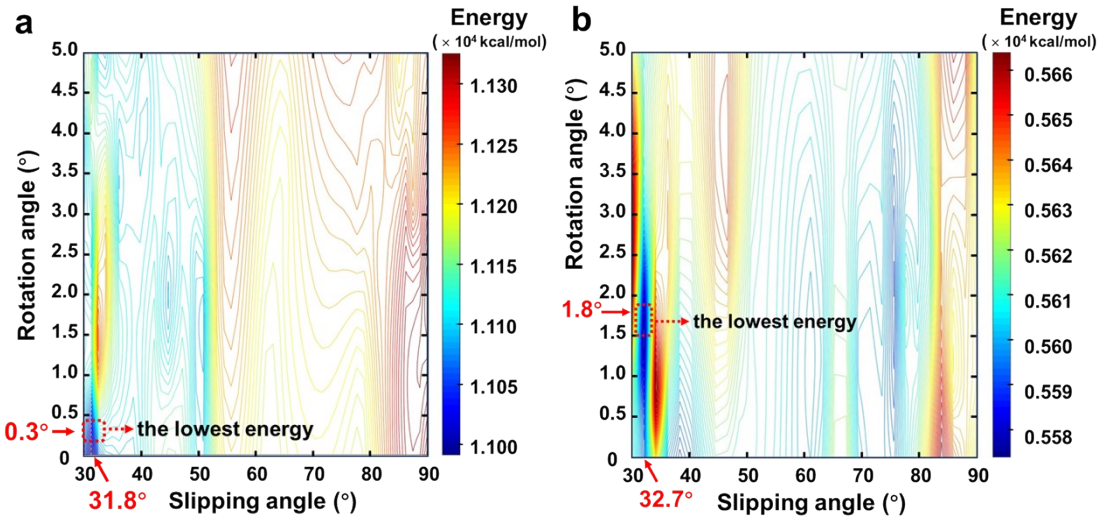

Figure S24. Dependence of energy of aggregates of 4-BBT-OPE$_3$ with two-column (a) and single-column (b) packing mode on slipping (θ_S) and rotation (θ_R) angles obtained by simulation with Material Studio 7.0 using COMPASS force field. The lowest energy of a single molecule in the optimal configuration of two-column packing mode was 1381.6 kcal/mol, about 12 kcal/mol lower than that of single-column packing mode (1393.7 kcal/mol).

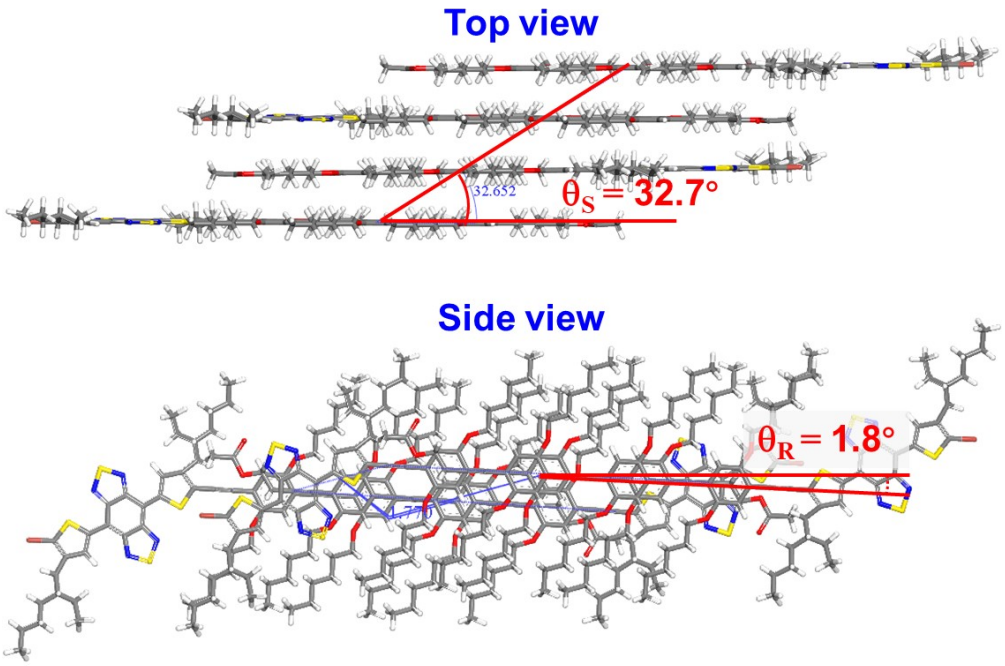

Figure S25. Single-column tetrameric packing mode of 4-BBT-OPE$_3$ with the lowest energy configuration simulated by Material Studio 7.0 using COMPASS force field.

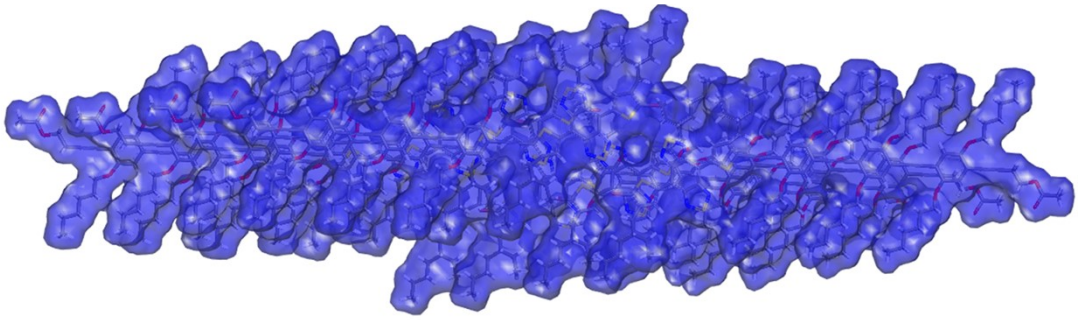

Packing modes	Total surface area of the packing modes (Å^2)	Number of molecules of the packing modes	Surface area of a single molecule (Å^2)	Overlapping area (Å^2/per molecule)
Two column	11389.92	8	1809.63	385.9
Single column	6141.24	4	1809.63	274.3

Connolly method: Overlapping area = (Surface area of a single molecule) – (Total surface area of the molecular assembly/Number of molecules).

Figure S26. Comparison of overlapping area between two-column and single- column packing models.

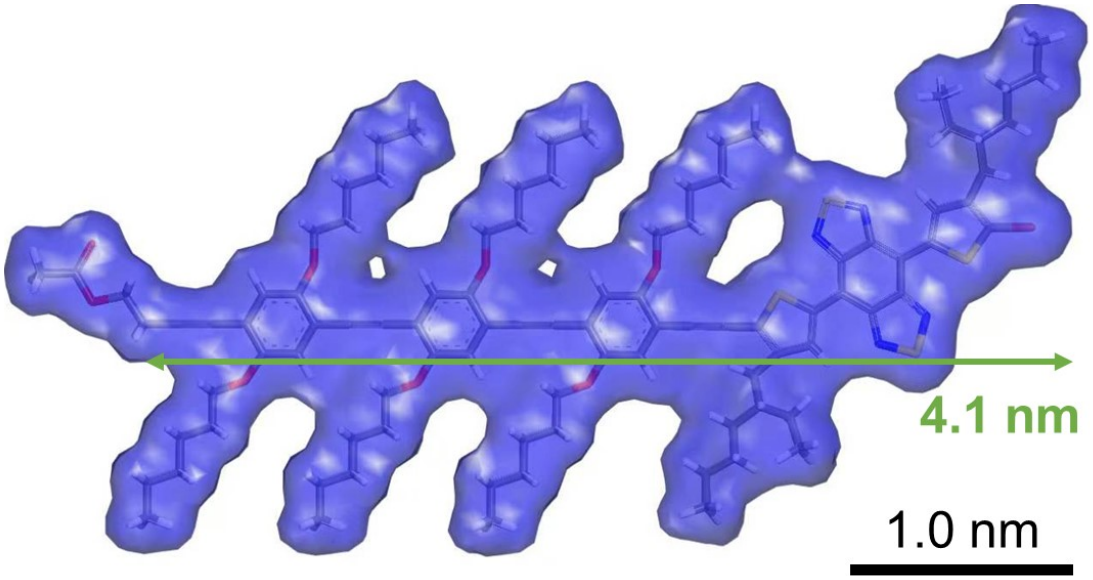

Figure S27. The theoretical length of conjugated segment in 4-BBT-OPE$_3$.

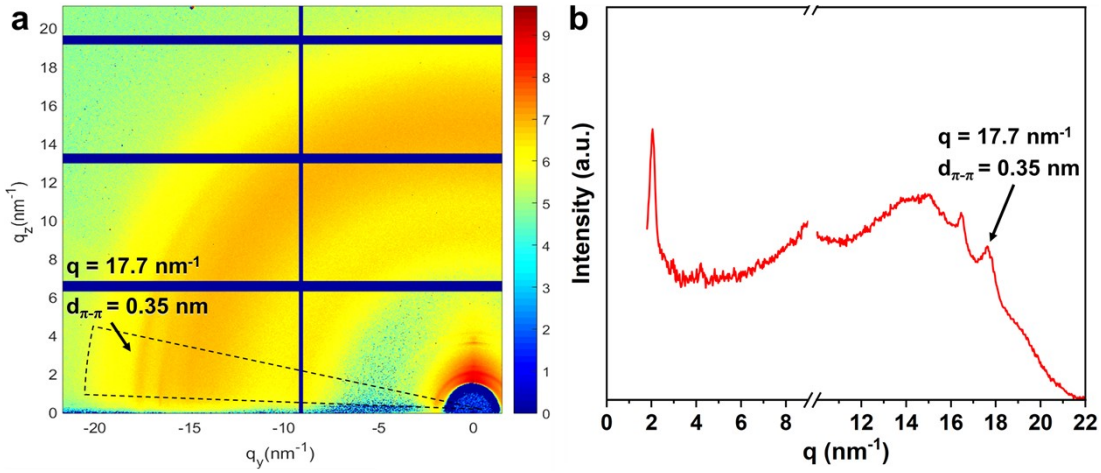

Figure S28. (a) 2D-GIWAXS pattern of the film of micelles of 4-BBT-OPE$_3$-*b*-P2VP$_{22}$. (b) 1D intensity profile along the q_y direction of 2D-GIWAXS pattern.

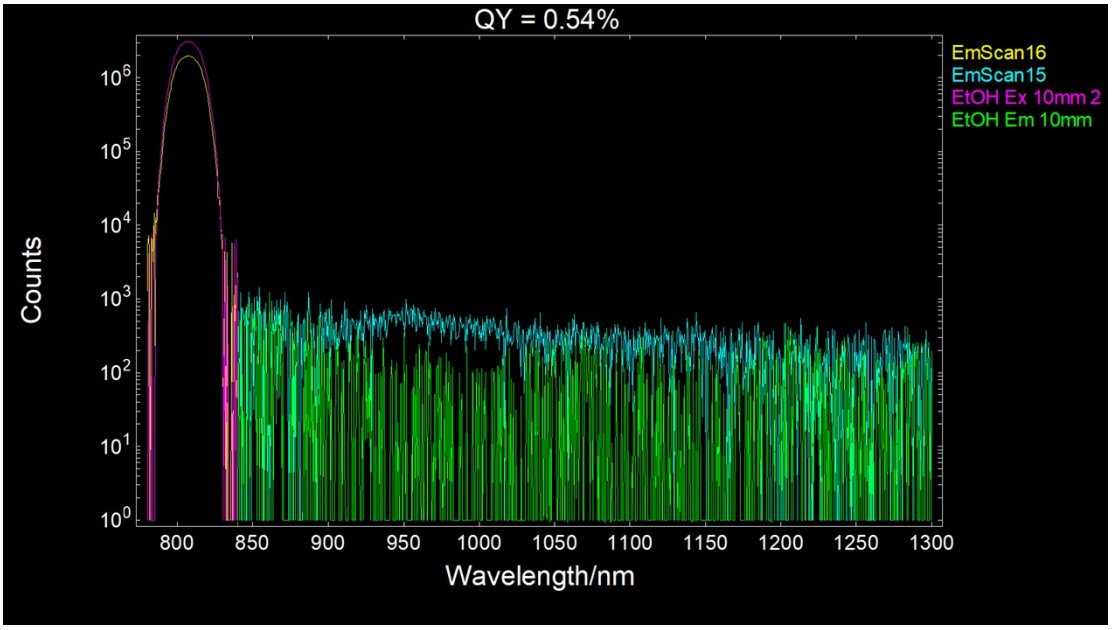

Figure S29. Photoluminescence emission spectra of fiber-like micellar solution of 4-BBT-OPE_3-*b*-$P2VP_{22}$ (0.1 mg/mL in ethanol) and pure ethanol. Φ_{PL} of micellar solution of 4-BBT-OPE_3-*b*-$P2VP_{22}$ was calculated to be about 0.5%.

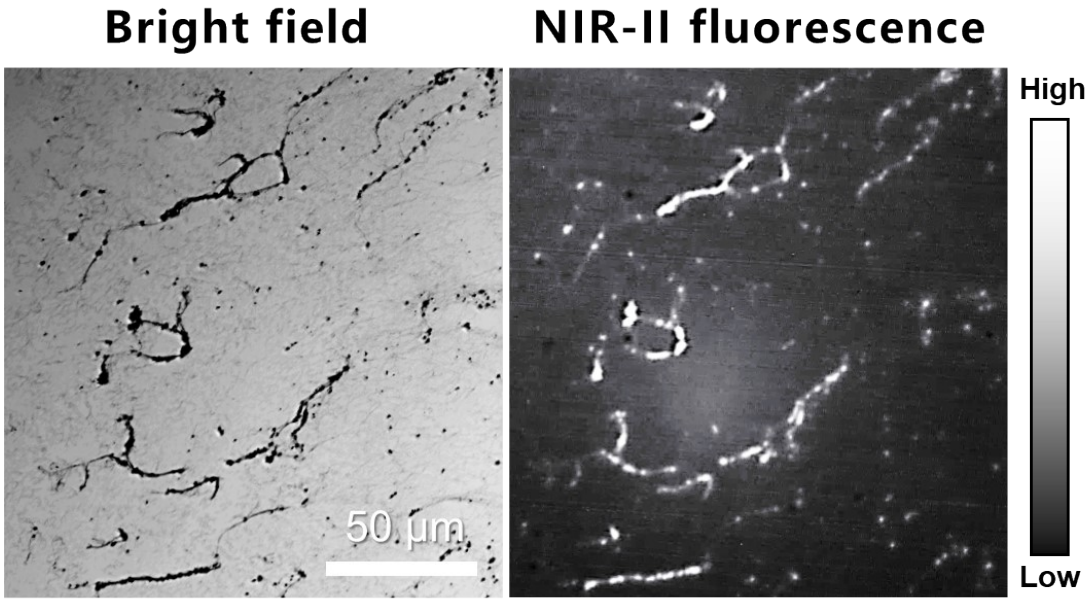

Figure S30. NIR-II fluorescence images of fiber-like micelles of 4-BBT-OPE_3-*b*-$P2VP_{22}$. NIR-II fluorescence imaging was carried out with an 808 nm laser excitation, a 20× objective. The images were taken by a NIRvana-LN camera, with a detection range of 900-1700 nm.

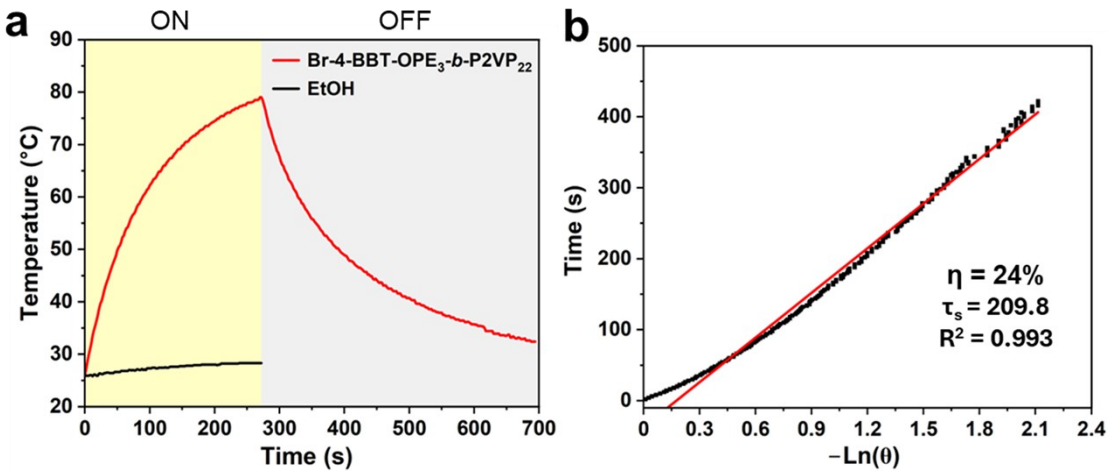

Figure S31. (a) Photothermal effect of 4-BBT-OPE_3-*b*-$P2VP_{22}$ micelles under 808 nm NIR laser irradiation (0.5 mg/mL, 1.68 W/cm^2). (b) Linear relationship between time and -Ln(θ) obtained from the cooling period of (a), and the photothermal conversion efficiency of 4-BBT-OPE_3-*b*-$P2VP_{22}$ can be calculated to be 24%.

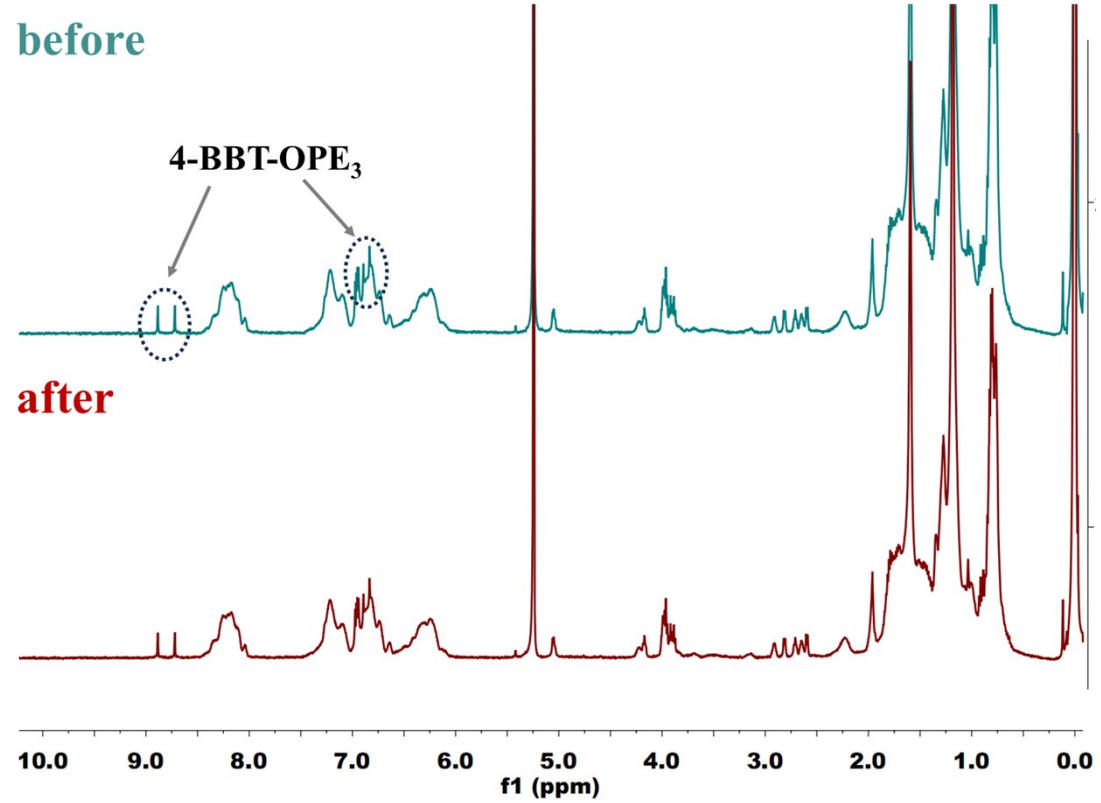

Figure 32. ^1H NMR spectra (CD_2Cl_2, 298 K, 500 MHz) of the block copolymer 4-BBT-OPE_3-*b*-$P2VP_{22}$ before and after NIR (808 nm, 1.02 W/cm^2) irradiation for a total of 23 min over five intervals.

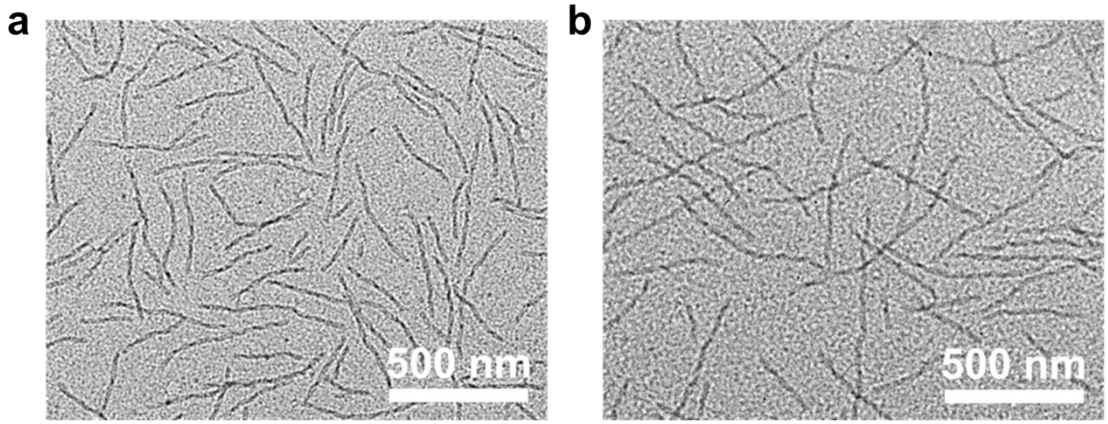

Figure S33. (a) TEM image of micelles of 4-BBT-OPE$_3$-*b*-P2VP$_{22}$ (0.5 mg/mL) formed by heating/cooling protocol, before 808 nm NIR laser irradiation. (b) TEM image of micelles of 4-BBT-OPE$_3$-*b*-P2VP$_{22}$ (0.5 mg/mL) after NIR laser irradiation five times (1.68 W/cm^2) and then cooling/aging at 25°C for 48 h. The morphology of micelles can be maintained, showing excellent stability of 4-BBT-OPE$_3$-*b*-P2VP$_{22}$ against NIR laser irradiation.

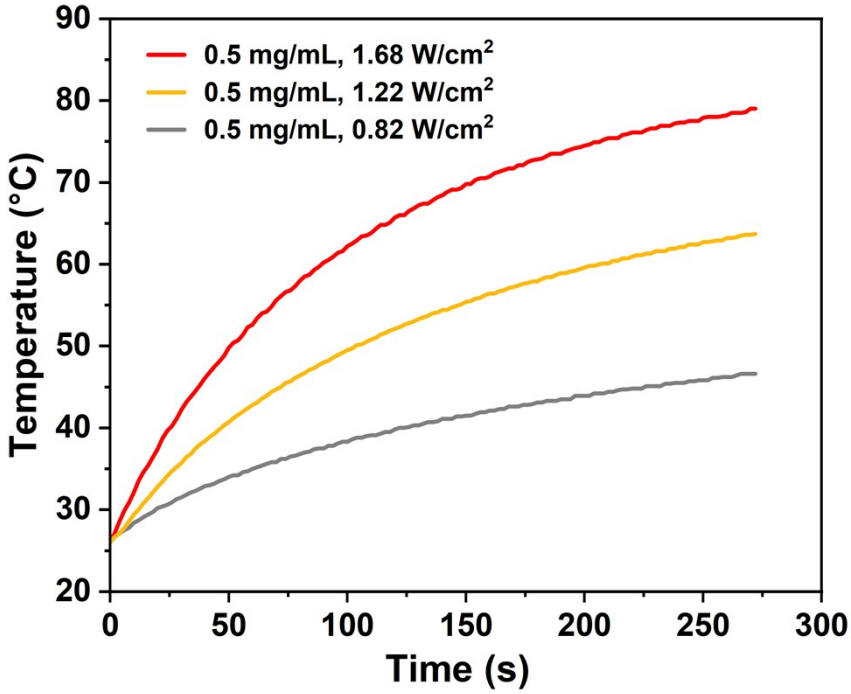

Figure S34. Photothermal effect of 4-BBT-OPE$_3$-*b*-P2VP$_{22}$ micelles (0.5 mg/mL) under 808 nm NIR laser irradiation with different power density.

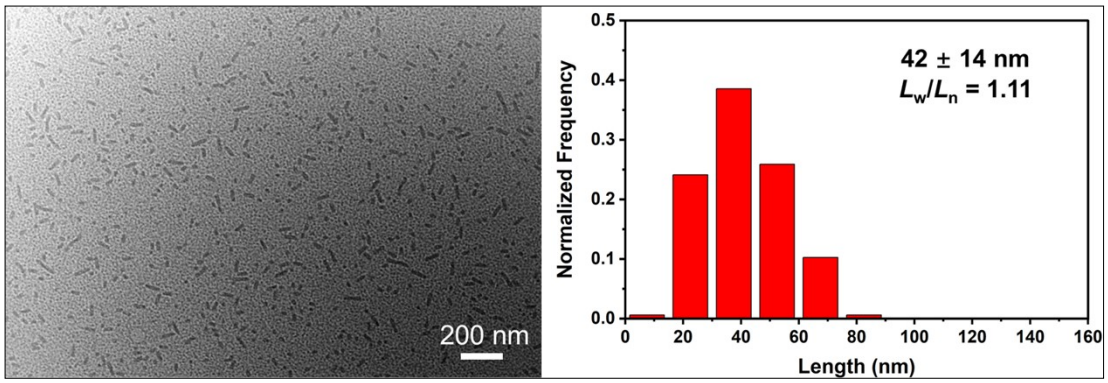

Figure S35. TEM image and contour length distribution histogram of seed micelles of 4-BBT-OPE$_3$-*b*-P2VP$_{22}$.

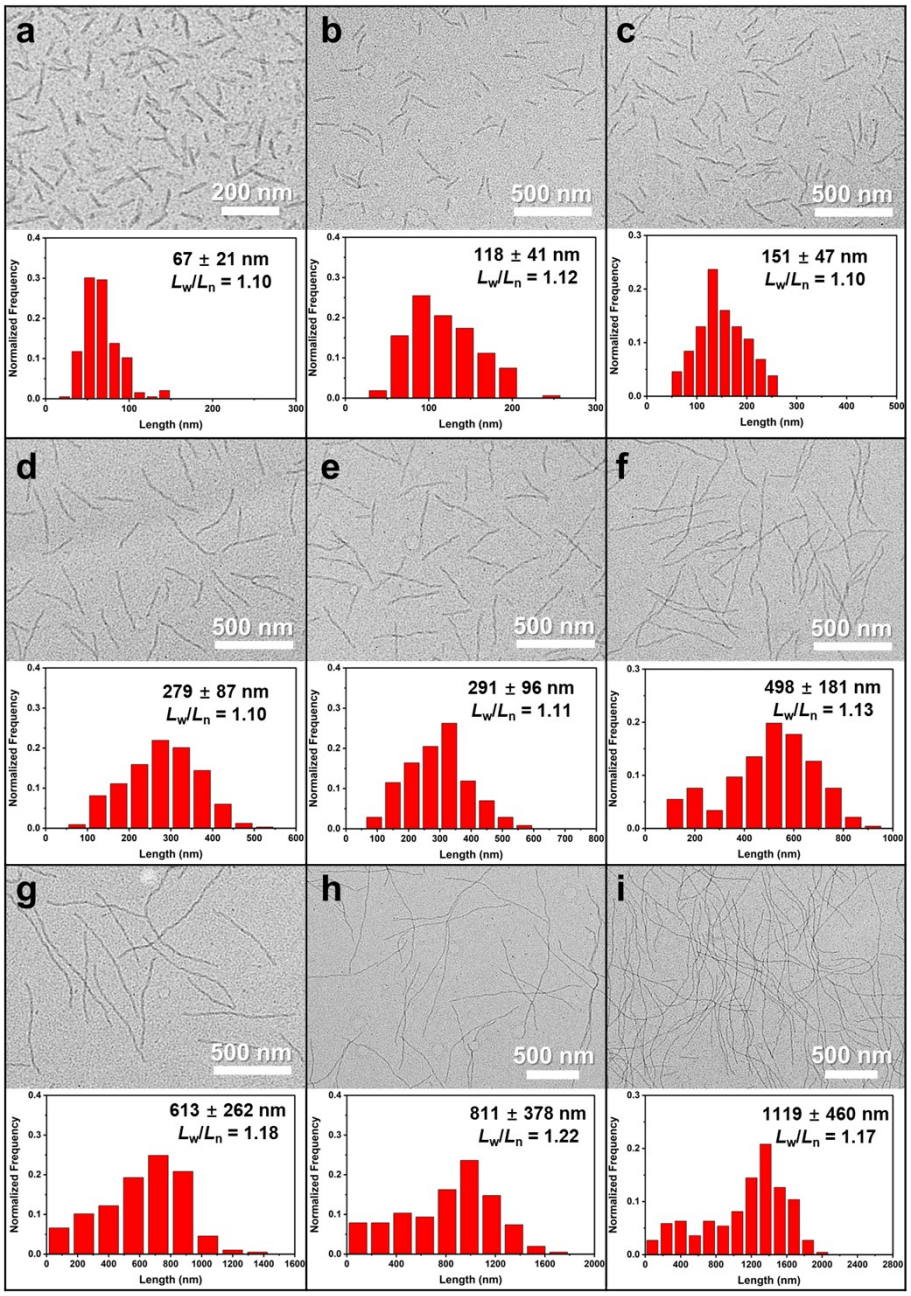

Figure S36. TEM images and contour length distribution histograms of fiber-like micelles of 4-BBT-OPE_3-*b*-$P2VP_{22}$ obtained by NIR light irradiation regulated self-seeding (0.1 mg/mL) with different time of NIR irradiation (1.68 W/cm^2). The seeds (0.1 mg/mL in ethanol) were irradiated by 808 nm laser for (a) 38 s (32°C), (b) 46 s (33°C), (c) 54 s (34°C), (d) 62 s (35°C), (e) 74 s (36°C), (f) 84 s (37°C), (g) 94 s (38°C), (h) 108 s (39°C) and (i) 120 s (40°C), respectively, followed by aging at room temperature for 48 h.

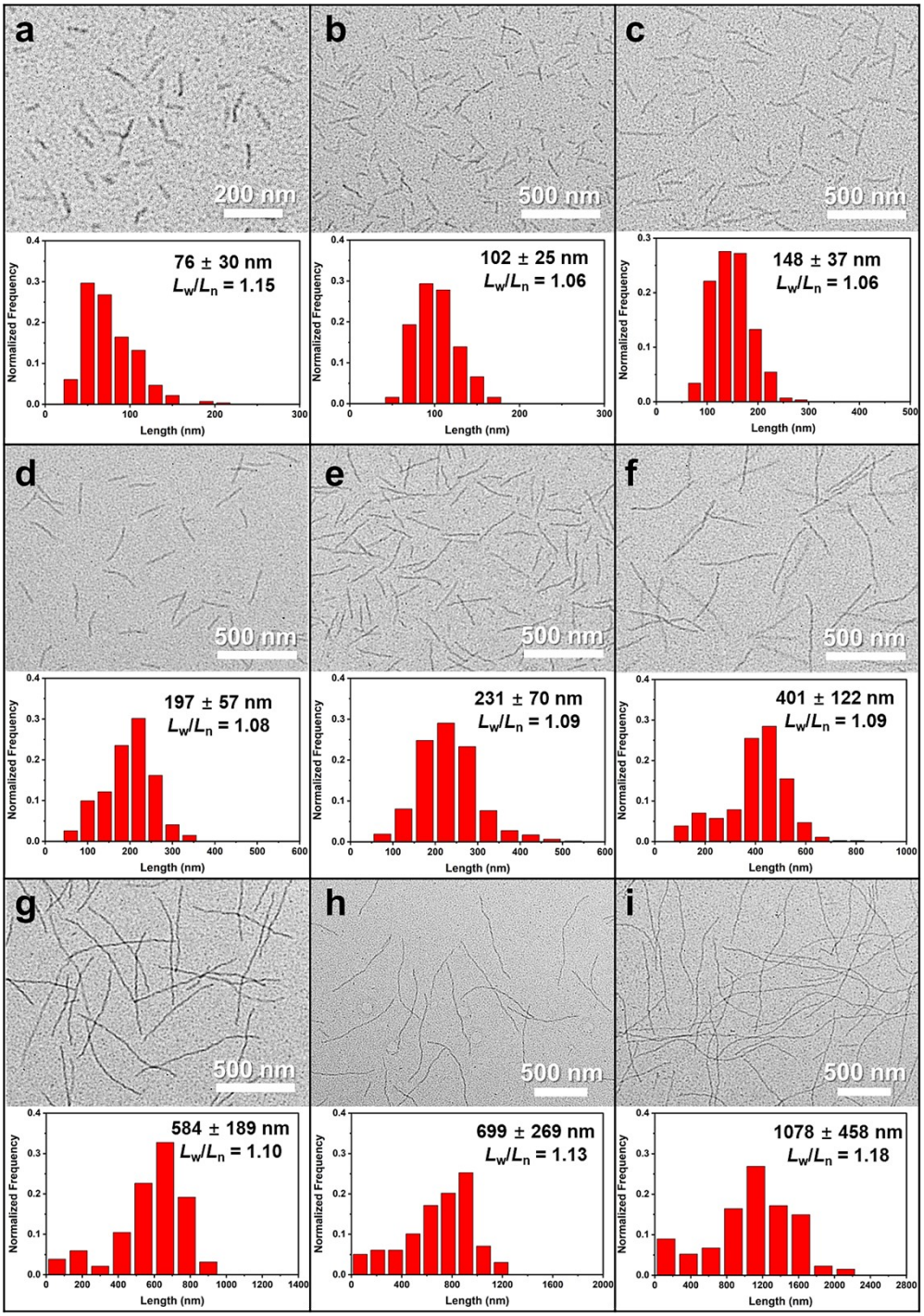

Figure S37. TEM images and contour length distribution histograms of fiber-like micelles of 4-BBT-OPE$_3$-*b*-P2VP$_{22}$ obtained by direct heating regulated self-seeding. The seeds (0.1 mg/mL in ethanol) were annealed at (a) 32°C, (b) 33°C, (c) 34°C, (d) 35°C, (e) 36°C, (f) 37°C, (g) 38°C, (h) 39°C and (i) 40°C for 30 min, respectively, followed by aging at room temperature for 48 h.

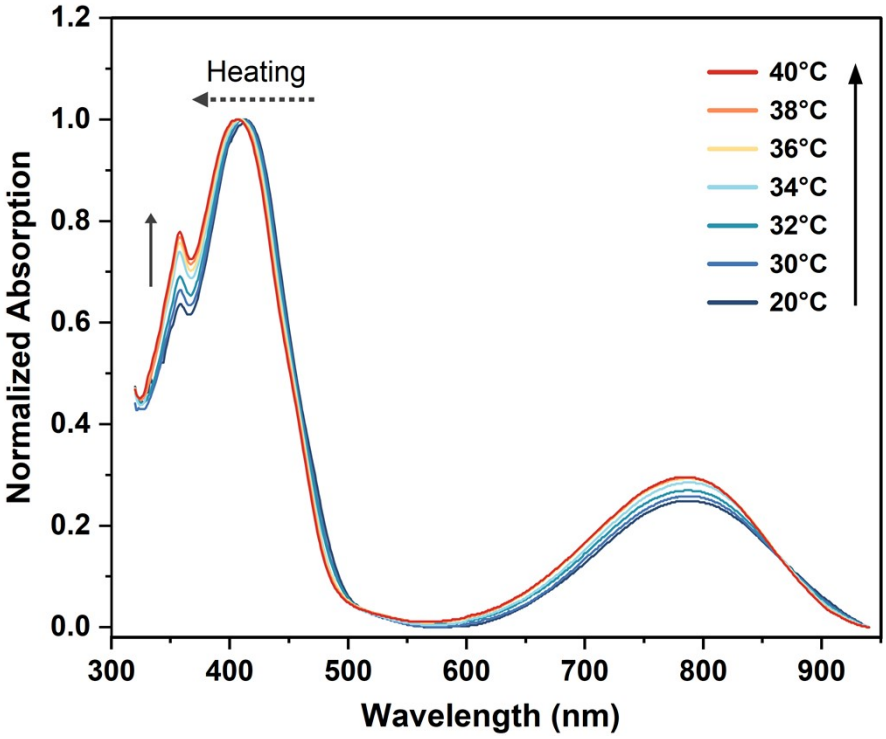

Figure S38. Temperature-dependent UV-vis-NIR absorption spectra of the seed micelles of 4-BBT-OPE$_3$-*b*-P2VP$_{22}$ in ethanol (0.1 mg/mL).

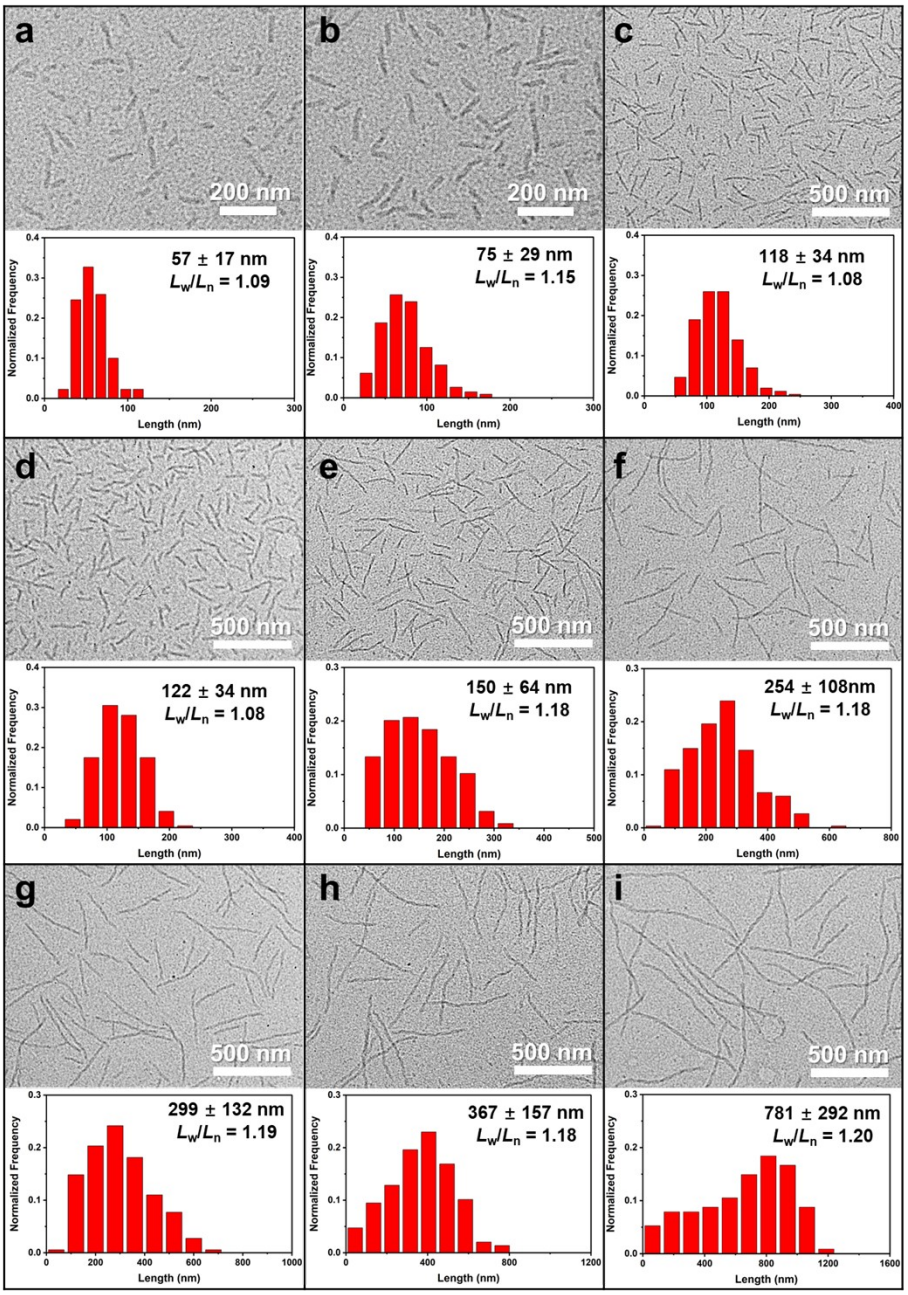

Figure S39. TEM images and contour length distribution histograms of fiber-like micelles of 4-BBT-OPE_3-*b*-$P2VP_{22}$ obtained by NIR light irradiation regulated self-seeding (0.2 mg/mL) with different time of NIR irradiation (1.68 W/cm^2). The seeds (0.2 mg/mL in ethanol) were irradiated by 808 nm laser for (a) 20 s (32°C), (b) 24 s (33°C), (c) 28 s (34°C), (d) 32 s (35°C), (e) 34 s (36°C), (f) 40 s (37°C), (g) 44 s (38°C), (h) 48 s (39°C) and (i) 52 s (40°C), respectively, followed by aging at room temperature for 48 h.

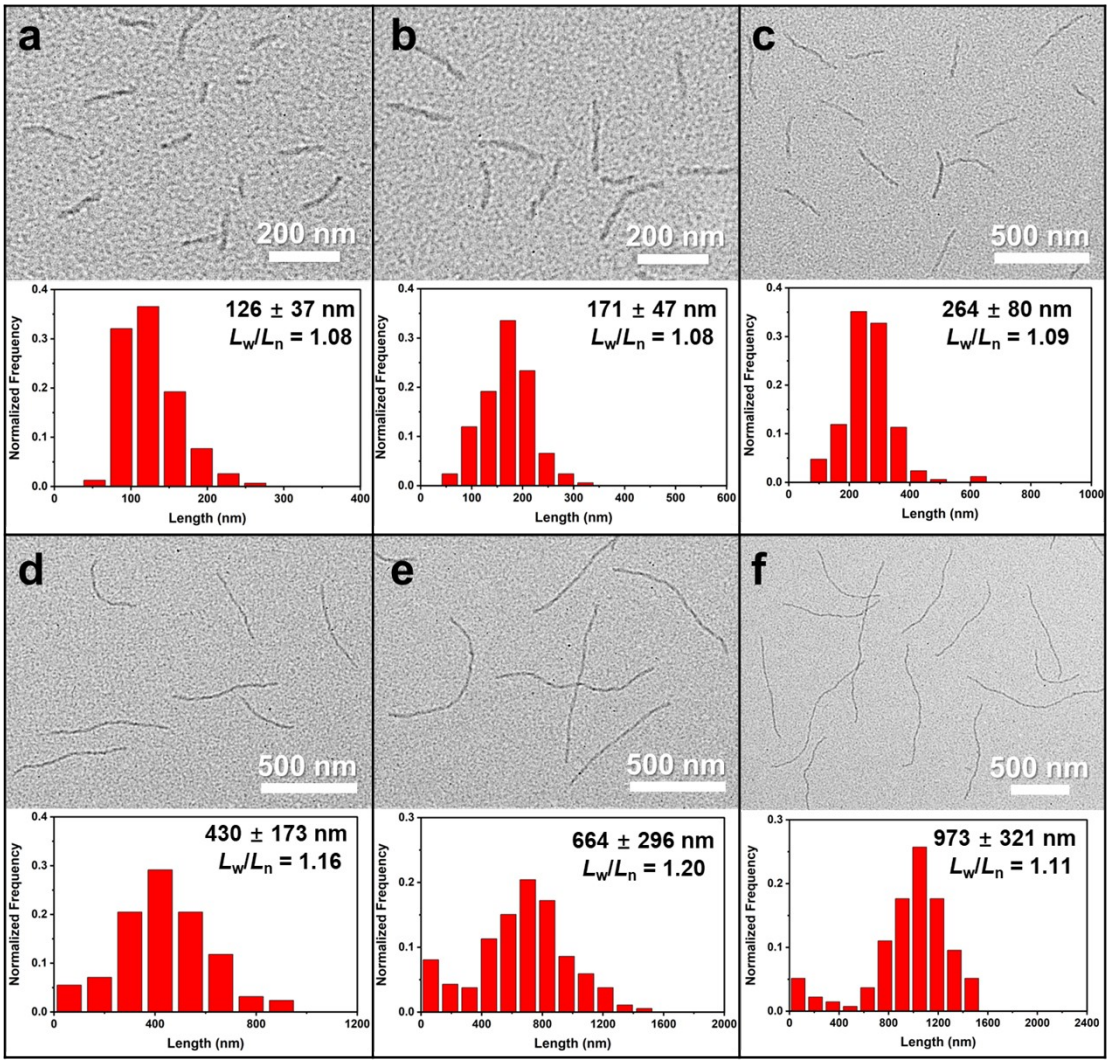

Figure S40. TEM images and contour length distribution histograms of fiber-like micelles of 4-BBT-OPE_3-*b*-$P2VP_{22}$ obtained by NIR light irradiation regulated self-seeding (0.05 mg/mL) with different time of NIR irradiation (1.68 W/cm^2). The seeds (0.05 mg/mL in ethanol) were irradiated by 808 nm laser for (a) 80 s (32°C), (b) 100 s (33°C), (c) 125 s (34°C), (d) 145 s (35°C), (e) 175 s (36°C) and (f) 200 s (37°C), respectively, followed by aging at room temperature for 48 h.

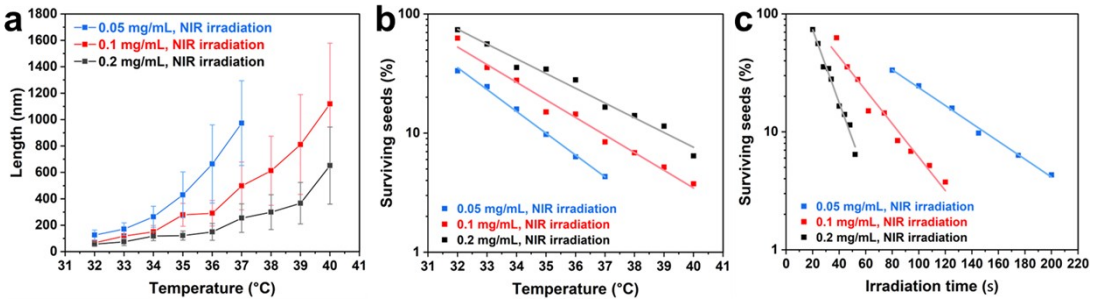

Figure S41. Dependence of (a) L_n of micelles of 4-BBT-OPE$_3$-*b*-P2VP$_{22}$ and (b) fraction of surviving seeds on annealing temperature, (c) dependence of fraction of surviving seeds micelles on irradiation time, obtained by NIR light regulated self-seeding with different contents of seed micelles (1.68 W/cm^2).

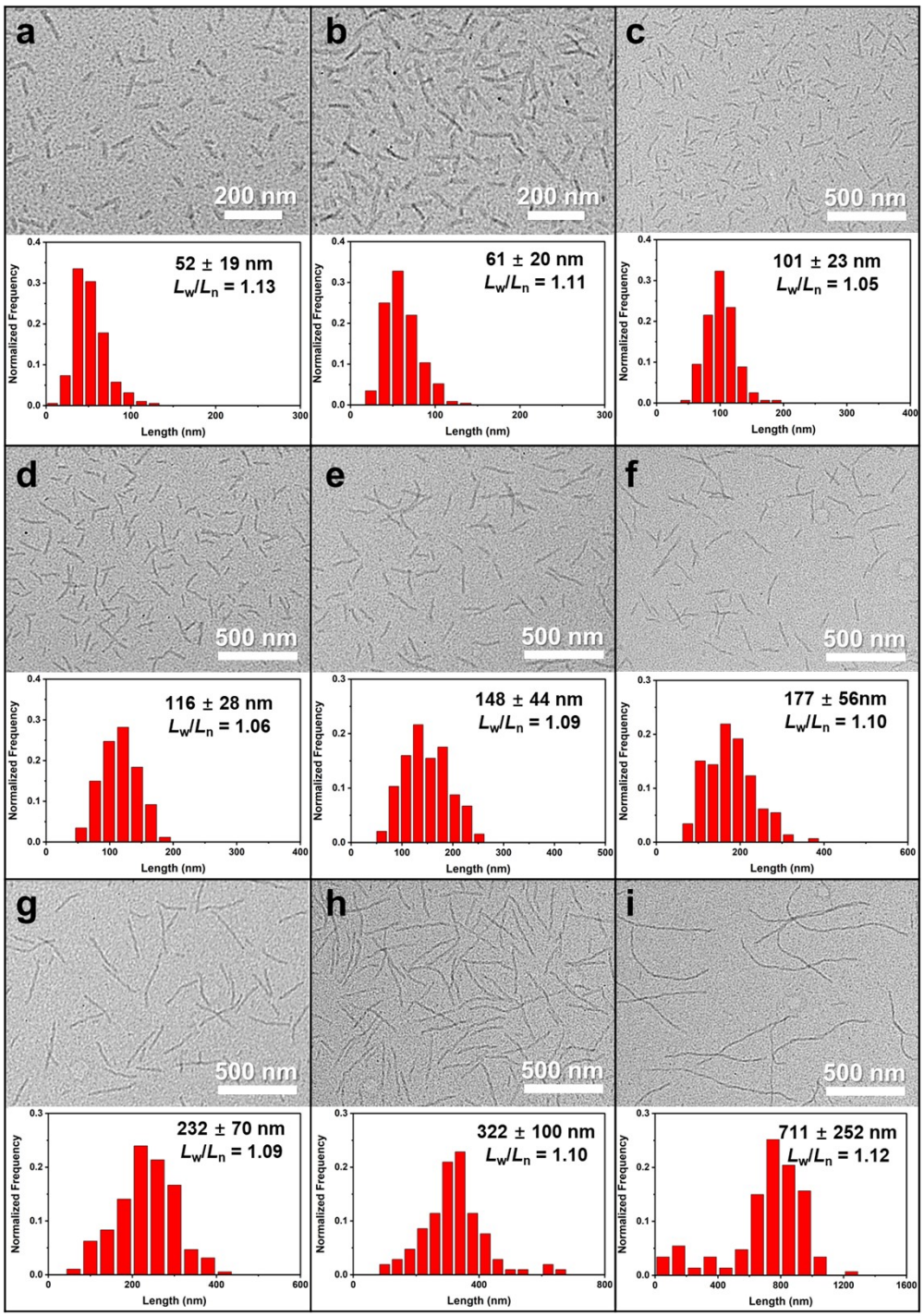

Figure S42. TEM images and contour length distribution histograms of fiber-like micelles of 4-BBT-OPE$_3$-*b*-P2VP$_{22}$ obtained by direct heating regulated self-seeding. The seeds (0.2 mg/mL in ethanol) were annealed at (a) 32^{o}C, (b) 33^{o}C, (c) 34^{o}C, (d) 35^{o}C, (e) 36^{o}C, (f) 37^{o}C, (g) 38^{o}C, (h) 39^{o}C and (i) 40^{o}C for 30 min, respectively, followed by aging at room temperature for 48 h.

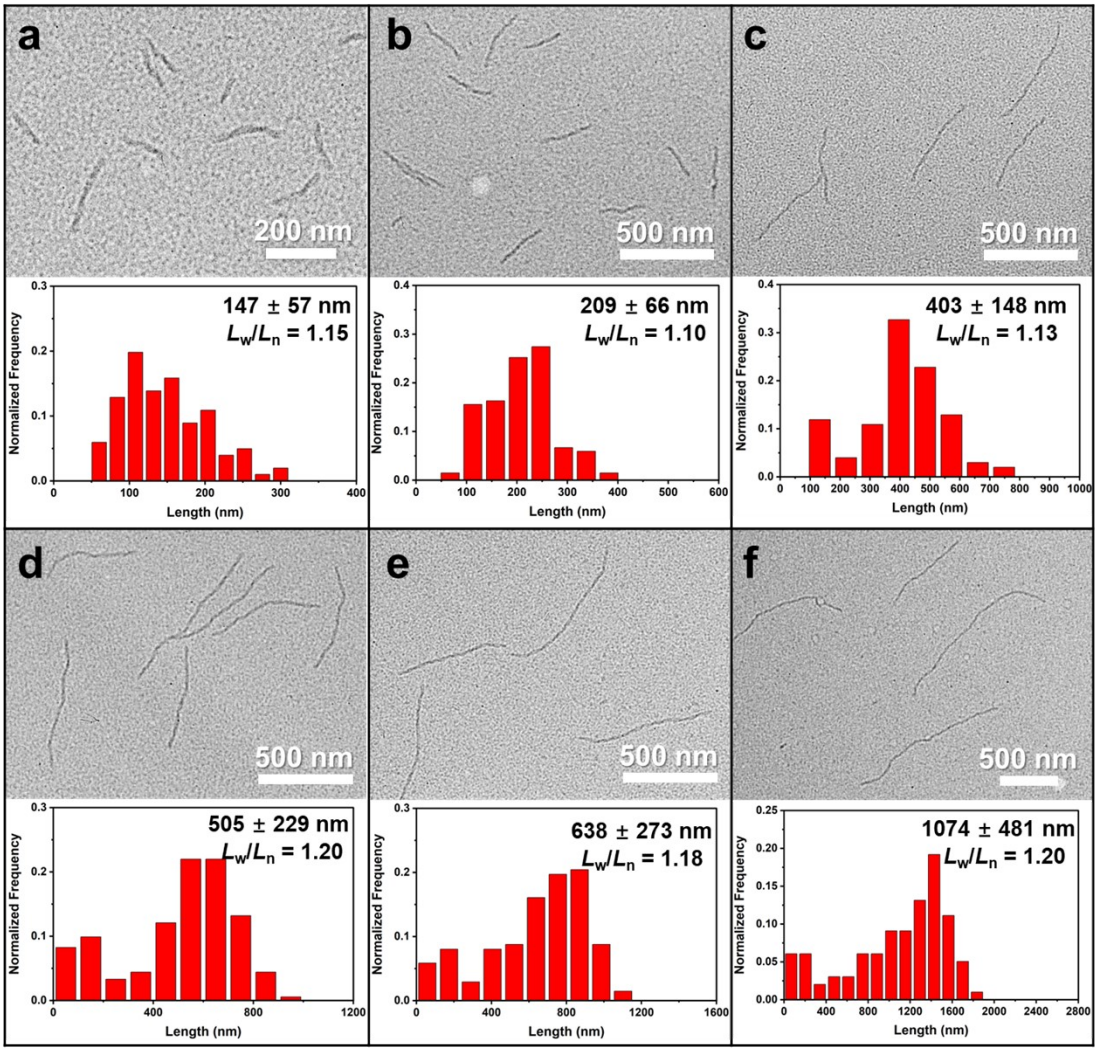

Figure S43. TEM images and contour length distribution histograms of fiber-like micelles of 4-BBT-OPE_3-*b*-$P2VP_{22}$ obtained by direct heating regulated self-seeding. The seeds (0.05 mg/mL in ethanol) were annealed at (a) 32°C, (b) 33°C, (c) 34°C, (d) 35°C, (e) 36°C and (f) 37°C for 30 min, respectively, followed by aging at room temperature for 48 h.

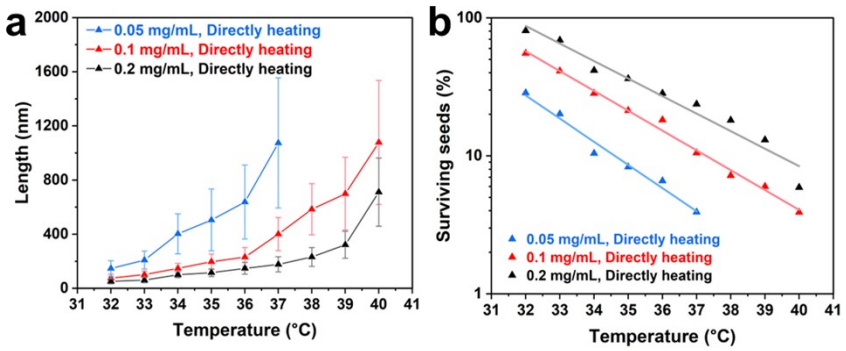

Figure S44. Dependence of (a) L_n of micelles of 4-BBT-OPE$_3$-*b*-P2VP$_{22}$ and (b) fraction of surviving seeds on annealing temperature obtained by direct heating regulated self-seeding with different contents of seed micelles.

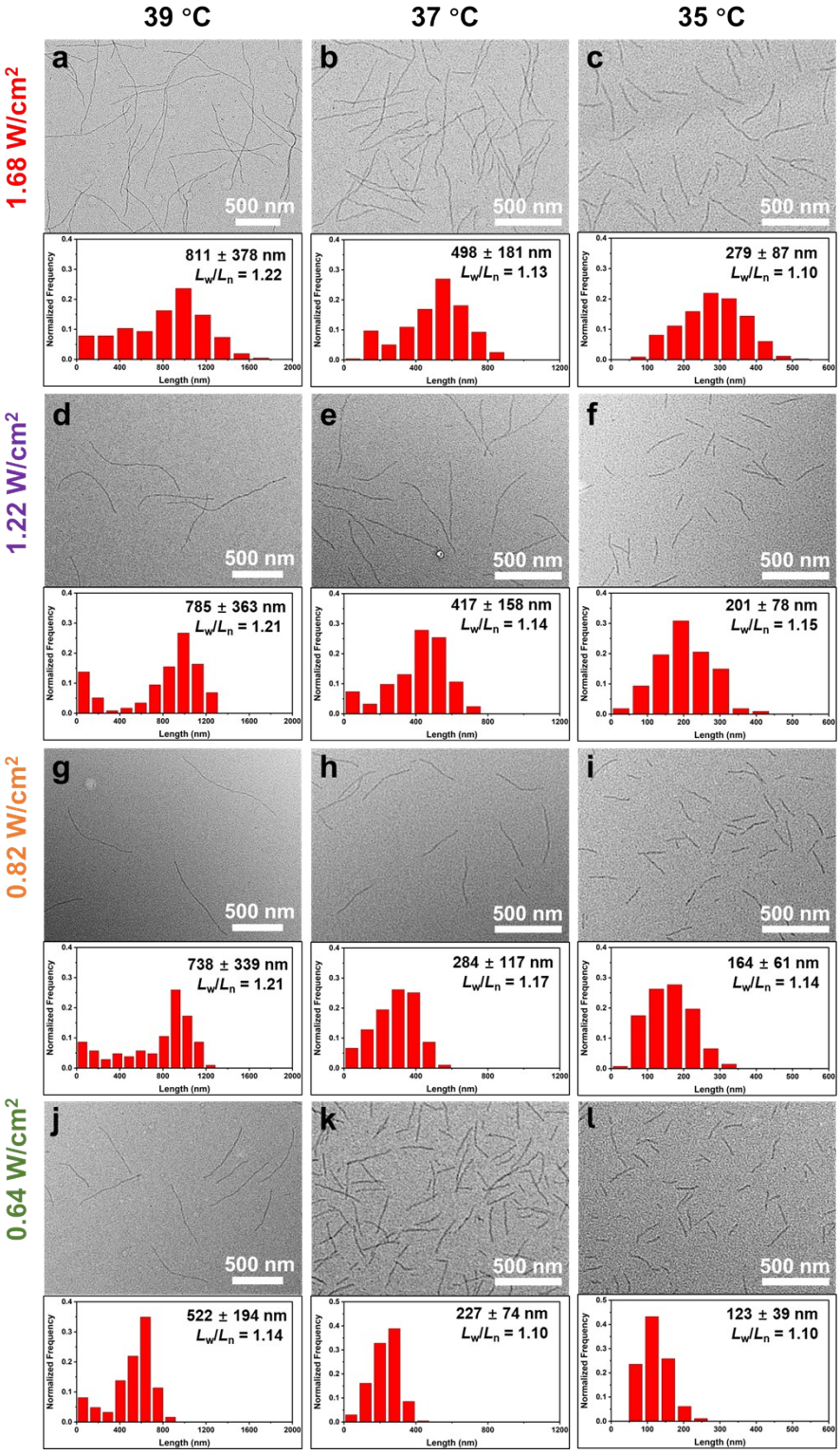

Figure S45. TEM images and contour length distribution histograms of fiber-like micelles of 4-BBT-OPE$_3$-*b*-P2VP$_{22}$ obtained by NIR light irradiation regulated self-seeding (0.1 mg/mL) with different power density. The seeds (0.1 mg/mL in ethanol) were irradiated by 808 nm laser with the power density of (a-c) 1.68, (d-f) 1.22, (g-i) 0.82 and (j-l) 0.64 W/cm^2 for different time to let the temperature of solution reached 39℃, 37℃ and 35℃, respectively, followed by aging at room temperature for 48 h.

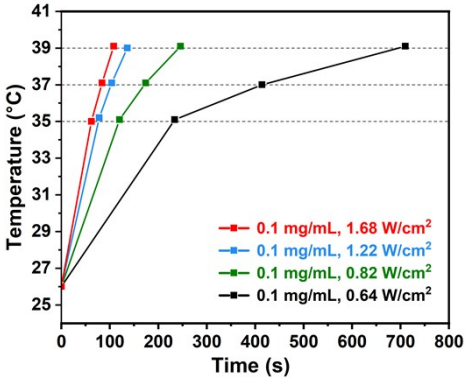

Figure S46. Curves showing the relationship between the temperature of the seed micellar solutions and the irradiation times under different powers.

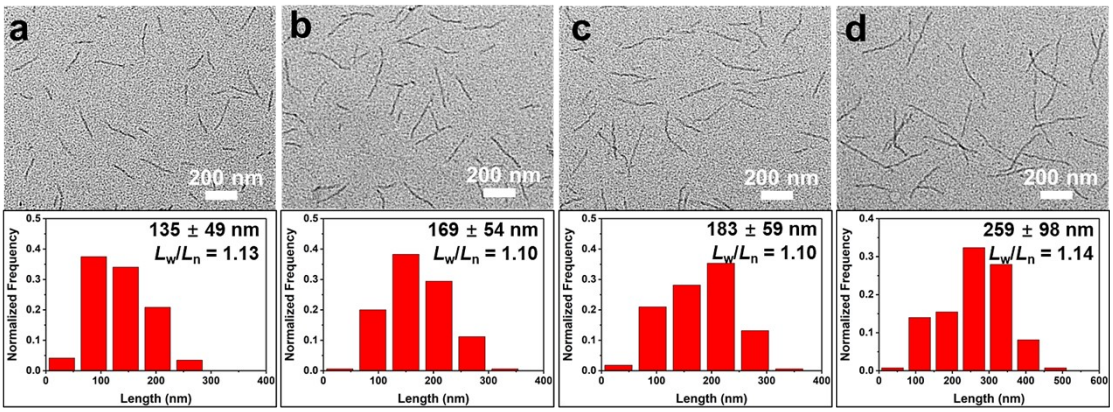

Figure S47. TEM images and contour length distribution histograms of fiber-like micelles of 4-BBT-OPE$_3$-*b*-P2VP$_{22}$ obtained by direct heating regulated self-seeding. The seed micellar solutions (0.1 mg/mL in ethanol) were heated from 26℃ to 37℃ by directly heating with heating rates of (a) 0.9℃/min, (b) 1.2℃/min, (c) 1.8℃/min and (d) 3.7℃/min, followed by cooling/aging at 25℃ for 48 h.

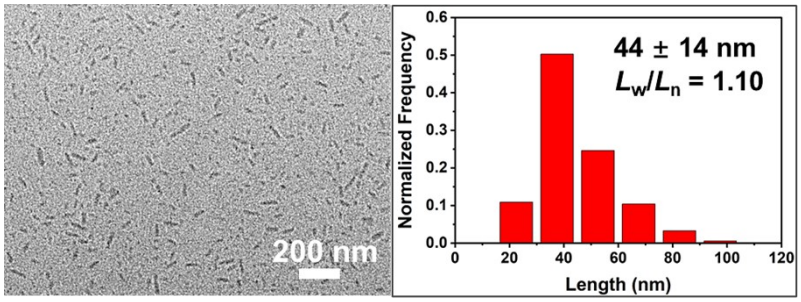

Figure S48. TEM image and contour length distribution histogram of seed micelles (0.05 mg/mL in ethanol) of OPV$_5$-*b*-P2VP$_{42}$. OPV$_5$-*b*-P2VP$_{42}$ diblock copolymer was the same sample described in a precious report.[1]

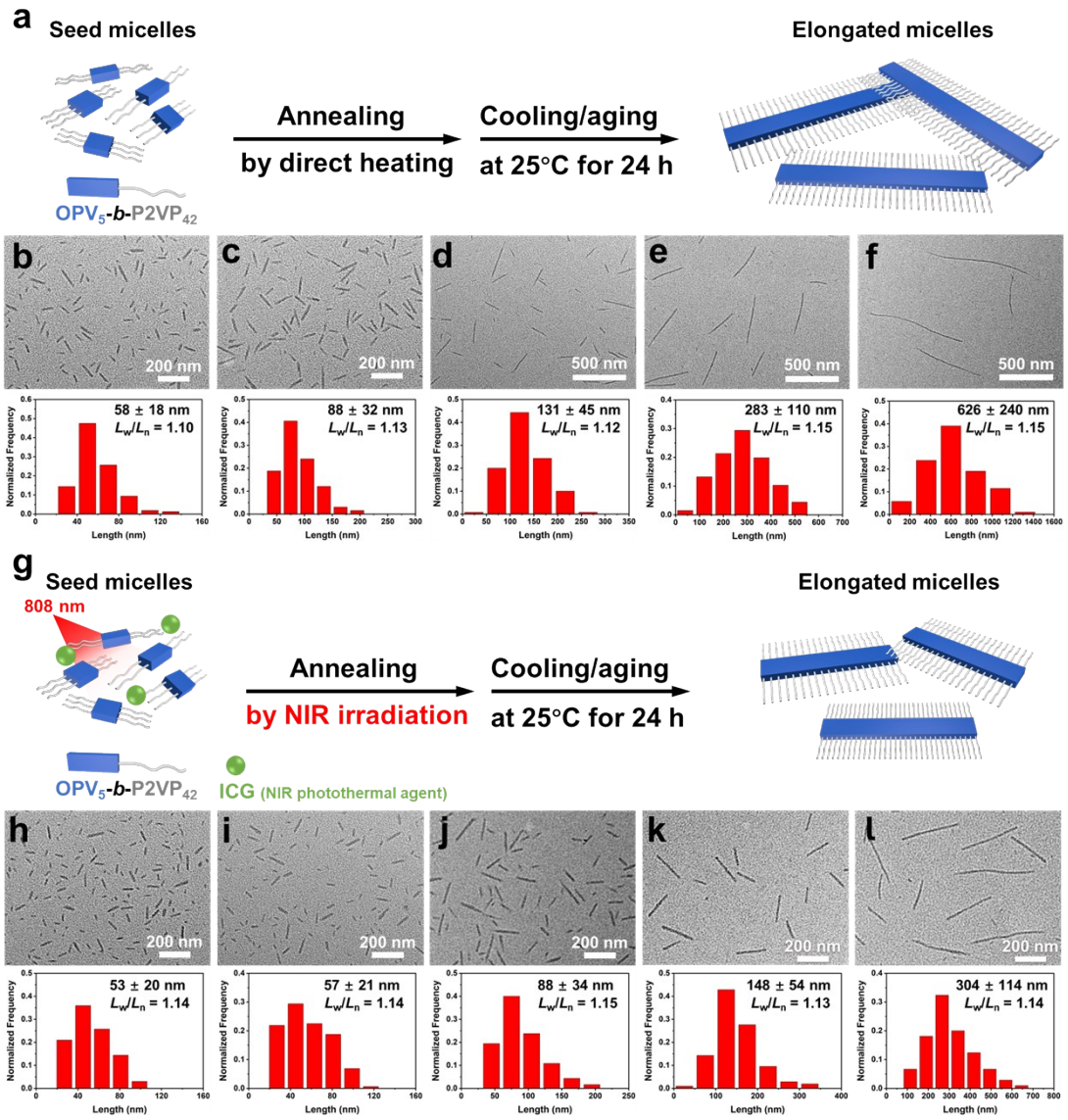

Figure S49. Schematic illustration of (a) direct heating regulated self-seeding and (g) NIR light regulated self-seeding of OPV_5-*b*-$P2VP_{42}$ with the presence of ICG. TEM images and contour length distribution histograms of fiber-like micelles of OPV_5-*b*-$P2VP_{42}$ obtained by direct heating regulated self-seeding or NIR light regulated self-seeding. The seeds (0.05 mg/mL in ethanol) were annealed at (b) 35°C, (c) 40°C, (d) 45°C, (e) 50°C and (f) 55°C for 30 min, respectively, followed by aging at room temperature for 24 h. The seeds (0.05 mg/mL in ethanol) with the presence of ICG (0.01 mg/mL) were irradiated by 808 nm laser (1.68 W/cm^2) for (h) 20 s (35 °C), (i) 28 s (40 °C), (j) 40 s (45 °C), (k) 58 s (50 °C) and (l) 112 s (55 °C), respectively, followed by aging at room temperature for 24 h.

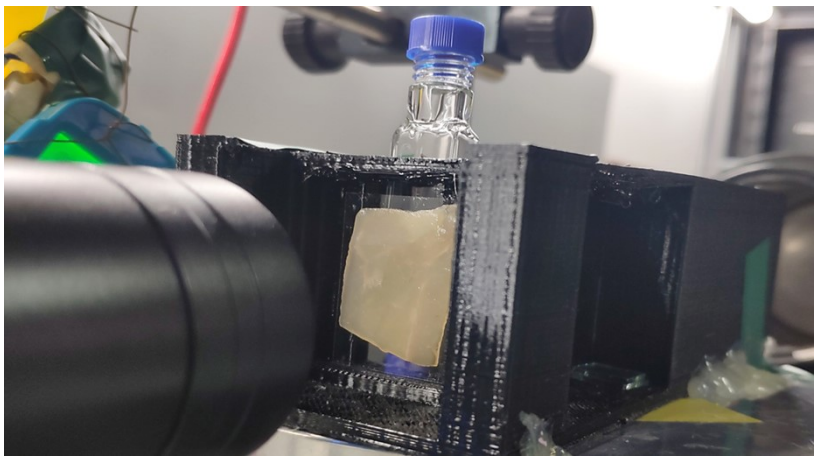

Figure S50. The experimental setup of NIR light regulated self-seeding of 4-BBT-OPE_3-*b*-$P2VP_{22}$ in the presence of blocking biological tissue.

Supporting tables

Table S1. Characteristics of homopolymer, oligomers and diblock copolymer in this article

sample	M_n^{GPC} (g/mol)[a]	M_n^{NMR} (g/mol)[b]	$Đ$ (GPC)[a]
4-BBT-OPE_3-OH	2100	-	1.01
4-BBT-OPE_3-alkyne	1700	-	1.01
N_3-$P2VP_{22}$	2900	2700	1.11
4-BBT-OPE_3-*b*-$P2VP_{22}$	5300	4400	1.08

[a] Determined by GPC using THF as eluent against polystyrene standards. [b] Calculated according to the *DP* of crystallized oligomer segment and corona chain determined by ^{1}H NMR on the basis of M_n of corresponding crystallized oligomer segment obtained from MALDI-TOF-MS.

Table S2. Characteristics of seed and elongated fiber-like micelles of 4-BBT-OPE_3-*b*-$P2VP_{22}$ obtained by NIR light regulated self-seeding in ethanol (0.10 mg/mL)[a]

irradiation[b] time (s)	T (°C)	L_n[c] (nm)	L_w[c] (nm)	L_w/L_n	σ[c] (nm)	σ/L_n
0	seed	42	46	1.11	14	0.34
38	32.2	67	74	1.10	21	0.31
46	33.2	118	132	1.12	41	0.35
54	34.1	151	165	1.10	47	0.31
62	35.0	279	306	1.10	87	0.31
74	36.1	291	323	1.11	96	0.33
84	37.1	498	564	1.13	181	0.36
94	38.0	613	724	1.18	262	0.43
108	39.1	811	987	1.22	378	0.47
120	40.1	1119	1307	1.17	460	0.41

[a] The mean length of micelles was calculated from measurements of over 100 individual micelles in multiple TEM images. [b] 808 nm laser, 1.68 W/cm^2. [c] L_n, L_w and σ are number- and weight-average micelle length, and standard deviation of micelle length distribution, respectively, as calculated from the histogram of length distribution.

Table S3. Characteristics of seed and elongated fiber-like micelles of 4-BBT-OPE_3-*b*-$P2VP_{22}$ obtained by NIR light regulated self-seeding in ethanol (0.20 mg/mL)[a]

irradiation time (s) [b]	T (°C)	L_n [c] (nm)	L_w [c] (nm)	L_w/L_n	σ [c] (nm)	σ/L_n
0	seed	42	46	1.11	14	0.34
20	32.1	57	62	1.09	17	0.31
24	33.4	75	86	1.15	29	0.39
28	34.2	118	128	1.08	34	0.29
32	35.2	122	131	1.08	34	0.28
34	35.9	150	178	1.18	64	0.43
40	37.2	254	300	1.18	108	0.43
44	38.3	299	357	1.19	132	0.44
48	39.1	367	434	1.18	157	0.43
52	39.8	652	781	1.20	292	0.45

[a] The mean length of micelles was calculated from measurements of over 100 individual micelles in multiple TEM images. [b] 808 nm laser, 1.68 W/cm^2. [c] L_n, L_w and σ are number- and weight-average micelle length, and standard deviation of micelle length distribution, respectively, as calculated from the histogram of length distribution.

Table S4. Characteristics of seed and elongated fiber-like micelles of 4-BBT-OPE$_3$-*b*-P2VP$_{22}$ obtained by NIR light regulated self-seeding in ethanol (0.05 mg/mL)[a]

irradiation[b] time (s)	T (°C)	L_n[c] (nm)	L_w[c] (nm)	L_w/L_n	σ[c] (nm)	σ/L_n
0	seed	42	46	1.11	14	0.34
80	32.3	126	136	1.08	37	0.29
100	33.1	171	184	1.08	47	0.28
125	34.1	264	288	1.09	80	0.30
145	35.1	430	499	1.16	173	0.40
175	36.0	664	795	1.20	296	0.45
200	37.0	973	1078	1.11	321	0.33

[a] The mean length of micelles was calculated from measurements of over 100 individual micelles in multiple TEM images. [b] 808 nm laser, 1.68 W/cm^2. [c] L_n, L_w and σ are number- and weight-average micelle length, and standard deviation of micelle length distribution, respectively, as calculated from the histogram of length distribution.

Table S5. Characteristics of seed and elongated fiber-like micelles of 4-BBT-OPE_3-*b*-$P2VP_{22}$ obtained by direct heating regulated self-seeding in ethanol (0.10 mg/mL)[a]

T[b] (°C)	L_n[c] (nm)	L_w[c] (nm)	L_w/L_n	σ[c] (nm)	σ/L_n
seed	42	46	1.11	14	0.34
32	76	88	1.15	30	0.39
33	102	108	1.06	25	0.24
34	148	158	1.06	37	0.25
35	197	213	1.08	57	0.29
36	231	252	1.09	70	0.30
37	401	438	1.09	122	0.30
38	584	645	1.10	189	0.32
39	699	791	1.13	269	0.39
40	1078	1271	1.18	458	0.42

[a] The mean length of micelles was calculated from measurements of over 100 individual micelles in multiple TEM images. [b] Annealing for 30 min at different temperature. [c] L_n, L_w and σ are number- and weight-average micelle length, and standard deviation of micelle length distribution, respectively, as calculated from the histogram of length distribution.

Table S6. Characteristics of seed and elongated fiber-like micelles of 4-BBT-OPE_3-*b*-$P2VP_{22}$ obtained by direct heating regulated self-seeding in ethanol (0.20 mg/mL)[a]

T[b] (°C)	L_n[c] (nm)	L_w[c] (nm)	L_w/L_n	σ[c] (nm)	σ/L_n
seed	42	46	1.11	14	0.34
32	52	59	1.13	19	0.36
33	61	68	1.11	20	0.33
34	101	106	1.05	23	0.23
35	116	123	1.06	28	0.24
36	148	160	1.09	44	0.30
37	177	195	1.10	56	0.32
38	232	253	1.09	70	0.30
39	322	353	1.10	100	0.31
40	711	800	1.12	252	0.35

[a] The mean length of micelles was calculated from measurements of over 100 individual micelles in multiple TEM images. [b] Annealing for 30 min at different temperature. [c] L_n, L_w and σ are number- and weight-average micelle length, and standard deviation of micelle length distribution, respectively, as calculated from the histogram of length distribution.

Table S7. Characteristics of seed and elongated fiber-like micelles of 4-BBT-OPE_3-*b*-$P2VP_{22}$ obtained by direct heating regulated self-seeding in ethanol (0.05 mg/mL)[a]

T[b] (°C)	L_n[c] (nm)	L_w[c] (nm)	L_w/L_n	σ[c] (nm)	σ/L_n
seed	42	46	1.11	14	0.34
32	147	168	1.15	57	0.39
33	209	230	1.10	66	0.31
34	403	457	1.13	148	0.37
35	505	608	1.20	229	0.45
36	638	754	1.18	273	0.43
37	1074	1288	1.20	481	0.45

[a] The mean length of micelles was calculated from measurements of over 100 individual micelles in multiple TEM images. [b] Annealing for 30 min at different temperature. [c] L_n, L_w and σ are number- and weight-average micelle length, and standard deviation of micelle length distribution, respectively, as calculated from the histogram of length distribution.

Table S8. Characteristics of elongated fiber-like micelles of 4-BBT-OPE$_3$-*b*-P2VP$_{22}$ obtained by NIR light regulated self-seeding (0.10 mg/mL) in ethanol using different power of 808 nm laser[a]

power (W/cm^2)	irradiation time (s)	T (°C)	L_n[c] (nm)	L_w[c] (nm)	L_w/L_n	σ[b] (nm)	σ/L_n
1.68	62	35.0	279	306	1.10	87	0.31
	84	37.1	498	564	1.13	181	0.36
	108	39.1	811	987	1.22	378	0.47
1.22	78	35.2	201	231	1.15	78	0.39
	104	37.1	417	476	1.14	158	0.38
	136	39.0	785	952	1.21	363	0.46
0.82	120	35.1	164	186	1.14	61	0.37
	174	37.1	284	332	1.17	117	0.41
	246	39.1	738	892	1.21	339	0.46
0.64	234	35.1	123	136	1.10	39	0.32
	414	37.0	227	251	1.10	74	0.32
	710	39.1	522	593	1.14	194	0.37

[a] The mean length of micelles was calculated from measurements of over 100 individual micelles in multiple TEM images. [b] L_n, L_w and σ are number- and weight-average micelle length, and standard deviation of micelle length distribution, respectively, as calculated from the histogram of length distribution.

Table S9. Characteristics of seed and elongated fiber-like micelles of 4-BBT-OPE_3-*b*-$P2VP_{22}$ obtained by NIR light regulated self-seeding (0.10 mg/mL) in the presence of blocking biological tissues with different thickness (1-4 mm)[a]

thickness (mm)	irradiation[b] time (min)	T (°C)	L_n[c] (nm)	L_w[c] (nm)	L_w/L_n	σ[c] (nm)	$σ/L_n$
1	2.8	38.2	434	469	1.08	125	0.29
2	3.8	38.1	303	329	1.08	89	0.29
3	6.7	38.0	251	272	1.09	74	0.29
4	7.9	38.3	220	241	1.10	69	0.31

[a] The mean length of micelles was calculated from measurements of over 100 individual micelles in multiple TEM images. [b] 808 nm laser, 1.68 W/cm^2. [c] L_n, L_w and σ are number- and weight-average micelle length, and standard deviation of micelle length distribution, respectively, as calculated from the histogram of length distribution.

Table S10. Characteristics of seed (0.05 mg/mL) and elongated fiber-like micelles of OPV_5-*b*-$P2VP_{42}$ obtained by direct heating regulated self-seeding in ethanol[a]

T[b] (°C)	L_n[c] (nm)	L_w[c] (nm)	L_w/L_n	σ[c] (nm)	σ/L_n
seed	44	49	1.10	14	0.32
35	58	64	1.10	18	0.31
40	88	99	1.13	32	0.36
45	131	146	1.12	45	0.34
50	283	325	1.15	110	0.39
55	626	717	1.15	240	0.38

[a] The mean length of micelles was calculated from measurements of over 100 individual micelles in multiple TEM images. [b] Annealing for 30 min at different temperature. [c] L_n, L_w and σ are number- and weight-average micelle length, and standard deviation of micelle length distribution, respectively, as calculated from the histogram of length distribution.

Table S11. Characteristics of seed (0.05 mg/mL) and elongated fiber-like micelles of OPV_5-*b*-$P2VP_{42}$ obtained by NIR light regulated self-seeding in ethanol with the presence of indocyanine green (ICG) (0.01 mg/mL)[a]

irradiation[b] time (s)	T (°C)	L_n[c] (nm)	L_w[c] (nm)	L_w/L_n	σ[c] (nm)	σ/L_n
0	seed	44	49	1.10	14	0.32
20	35.3	53	60	1.14	20	0.37
28	40.3	57	65	1.14	21	0.37
40	45.2	88	101	1.15	34	0.39
58	50.3	148	168	1.13	54	0.37
112	55.1	304	346	1.14	114	0.37

[a] The mean length of micelles was calculated from measurements of over 100 individual micelles in multiple TEM images. [b] 808 nm laser, 1.68 W/cm^2. [c] L_n, L_w and σ are number- and weight-average micelle length, and standard deviation of micelle length distribution, respectively, as calculated from the histogram of length distribution.

REFERENCES

1. Z. Wang, C. Ma, X. Huang, G. Lu, M. A. Winnik and C. Feng, *Macromolecules*, 2021, **54**, 6705-6717.
2. C. Würth, M. Grabolle, J. Pauli, M. Spieles and U. Resch-Genger, *Nat. Protoc.*, 2013, **8**, 1535-1550.
3. T. Chen, T. Yao, H. Peng, A. K. Whittaker, Y. Li, S. Zhu and Z. Wang, *Adv. Funct. Mater.*, 2021, **31**, 2106079.
4. D. Xi, M. Xiao, J. Cao, L. Zhao, N. Xu, S. Long, J. Fan, K. Shao, W. Sun, X. Yan and X. Peng, *Adv. Mater.*, 2020, **32**, 1907855.
5. H. Sun, *J. Phys. Chem. B*, 1998, **102**, 7338-7364.
6. H. Sun, P. Ren and J. R. Fried, *Comput. Theor. Polym. Sci.*, 1998, **8**, 229-246.
7. M. L. Connolly, *Science*, 1983, **221**, 709-713.
8. M. L. Connolly, *J. Appl. Crystallogr.*, 1983, **16**, 548-558.
9. L. Xiao, T. Xia, J. Zhang, S. J. Parkinson, J. Y. Rho, A. P. Dove and R. K. O' Reilly, *Nat. Synth.*, 2025, **4**, 808-815.
10. J. Nie, Z. Wang, X. Huang, G. Lu and C. Feng, *Macromolecules*, 2020, **53**, 6299-6313.
11. A. Elangovan, Y.-H. Wang and T.-I. Ho, *Org. Lett.*, 2003, **5**, 1841-1844.